Title

A fast and accurate modeling approach for water and steam thermodynamics with practical applications in district heating system simulation

Authors

Hinkelman, Kathryn

Anbarasu, Saranya

Wetter, Michael

et al.

Publication Date

2022-09-01

DOI

10.1016/j.energy.2022.124227

Peer reviewed

A Fast and Accurate Modeling Approach for Water and Steam Thermodynamics with Practical Applications in District Heating System Simulation

Kathryn Hinkelman[a], Saranya Anbarasu[b], Michael Wetter[c], Antoine Gautier[c], Wangda Zuo[a,d,*]

[a]*Architectural Engineering, Pennsylvania State University, University Park, 16802, PA, USA*
[b]*Civil, Environmental and Architectural Engineering, University of Colorado, Boulder, 80309, CO, USA*
[c]*Lawrence Berkeley National Laboratory, Berkeley, 94720, CA, USA*
[d]*National Renewable Energy Laboratory, Golden, 80401, CO, USA*

Abstract

In U.S. district heating (DH) systems, steam is the most common heat transport medium. Industry demand for new advanced modeling capabilities of complete steam DH systems is increasing; however, the existing models for water/steam thermodynamics are too slow for large system simulations because of computationally expensive algebraic loops that require the solution to nonlinear systems of equations. For practical applications, this work presents a novel split-medium approach that implements numerically efficient liquid water models alongside various water/steam models, breaking costly algebraic loops by decoupling mass and energy balance equations. New component models for steam DH systems are also presented. We implemented the models in the equation based Modelica language and evaluated accuracy and computing speed across multiple scales: from fundamental thermodynamic properties to complete districts featuring 10 to 200 buildings. Compared to district models with the IF97 water/steam model and equipment models from the Modelica Standard Library, the new implementation improves the scaling rate for large districts from cubic to quadratic with negligible compromise to accuracy. For an annual simulation with 180 buildings, this translates to a computing time reduction from 33 to 1-1.5 hours. These results are critically important for industry practitioners to simulate steam DH systems at large scales.

1. Introduction

1.1. Motivation

District heating (DH) can effectively reduce CO_2 emissions and enable communities to leverage economizes of scale benefits [1]. The global DH market is large, with an estimated 80,000 systems in operation that distribute hot water and steam through almost 600,000 km of distribution pipes [2]. In the United States, steam is the most common medium for DH, representing 97% of all installations [3]. Beyond heating buildings alone, steam DH provides beneficial waste-heat recovery opportunities when coupled with power plants (e.g., combined heat and power) or other industrial systems (e.g., wastewater treatment, metal refineries, etc.). While the conversion of steam DH systems (first generation) to hot water DH systems (second generation and later) is an important mechanism to realize deep carbon savings [2], high-quality energy such as steam will likely still be present in future energy grids due to its mutualistic benefits with power generation and high-heat industrial processes such as those listed in [4].

Modeling and simulation can improve the design and operation of DH systems while also aiding the transition of legacy steam-based systems to newer technologies. While many software tools can simulate individual buildings, the demand for district-scale simulations are rapidly increasing. This work is part of a larger collaborative project [5] involving the URBANopt software development kit [6] and the open-source Modelica Buildings Library (MBL) [7] to create district-scale software modeling tools for energy optimization, grid responsiveness, and waste-heat recovery. Because of the prevalence of steam in DH, combined heat and power (CHP) systems, and as waste-heat from industrial processes, it is imperative that these modeling tools are capable of simulating steam systems. In particular, steam DH simulation times need to be relatively fast for industry to adopt the computing tools in practice. To accomplish this task, the first step is to implement a modeling approach for water and steam thermodynamics that is fast and accurate for DH simulations at large scales.

1.2. Literature Review

Table 1 summarizes several water/steam models that can be considered typical examples of analytical models in scientific and industrial practices. The International Association for the Properties of Water and Steam (IAPWS) develops formulations for thermodynamic properties of water and steam for various applications. Based on the Helmholtz free energy, the IAPWS-95 model is a single-set of equations with density ρ and temperature T as independent variables; the model covers the largest

*Corresponding author.
Email address: wangda.zuo@psu.edu (Wangda Zuo)

Nomenclature

Abbreviations

c	condensate (generic)
CD	constant density liquid water
CHP	combined heat and power
CVRMSE	coefficient of variation of the root mean square error
DH	district heating
IAPWS	international association for the properties of water and steam
IAPWS95	scientific formulation for water/steam (Appendix A)
IF97	industrial formulation for water/steam (Appendix B)
MBL	Modelica Buildings Library
MSL	Modelica Standard Library
RMSE	root mean square error
S	simplified steam model (Appendix C)
s	steam (generic)
SBTL	spline-based table look-up
TDD	temperature dependent density liquid water

Accents

$\bar{}$	mean
$\dot{}$	flow rate
$\hat{}$	approximate

Parameters

δ	small number for regularization
$\mathcal{S}'$	pump performance data
a	regression coefficient
F	number of fluid ports
i	index
k	constant coefficient
N	number in series
n	number of operating points
p	scaling power

Subscripts

0	nominal
1	inlet port
2	outlet port
a	atmospheric
cpu	central processing unit
f	fuel
fg	vaporization
fl	flow
h	hydraulic
l	loss
m	motor
max	maximum
sat	saturated state
t	turbulent transition point

Variables

χ	vapor quality
Δp	change in pressure
η	efficiency
ρ	density
c_p	isobaric specific heat
c_v	isochoric specific heat
h	specific enthalpy
m	mass
P	electrical power
p	pressure
Q	heat
r	rotational speed
s	specific entropy
T	temperature
t	time
U	internal energy
V	volume
y	load ratio

range of conditions and is intended for scientific applications where accuracy is of utmost importance [8]. The IAPWS also released their industrial formulation (IF97) for water and steam that is based on the Gibbs free energy [9]; this model contains multiple equations corresponding to different regions of water and steam thermodynamics, and includes forward and backward equations with various combinations of independent variables: (p, T), (p, h), and (p, s), where p is pressure, h is specific enthlapy, and s is specific entropy. With this formulation, the computing time is typically faster than the IAPWS-95 model and produces negligibly small accuracy sacrifices. The IF97 model is by far the most widely adopted medium model for

Table 1: Representative analytical models for calculating water and steam thermodynamic properties.

Name	*Applicable Range(s)*		*Regions*[1]	*Intended*	*Freely*	*Ref.*
	p (MPa)	*T (°C)*		*Application*	*Available*	
IAPWS-95	0–1000	−22–1000	1–6	Scientific	Yes	[8]
IF97	0–100 800–2000	0–800 0–10	1–6 5	All Industrial High-temperature	Yes	[9]
Polynomial Fits with Splines	0.08–100	0–800	1–6	All Industrial	No	[10]
Polynomial Fits	0.01–100	0–800	1–6	All Industrial	No	[11]
Power Series with Log Transformations	0–21	0–370	2,4	All Industrial	Yes	[12]
MBL Constant Density (CD)[2]	0–4	–1–130	1	Building HVAC	Yes	[7]
MBL Temperature Dependent Density (TDD)[3]	0–4	–1–373	1	Building HVAC	Yes	[7]

[1] Region numbers correspond to: 1 subcooled liquid region, 2 saturated water line, 3 wet steam region, 4 dry saturated steam line, 5 superheated vapor region, and 6 supercritical region. See Figure 2 for graphical representation.
[2] Referred as *TemperatureDependentDensity* in the MBL [7].
[3] Referred as *Water* in the MBL [7].

simulation applications [13, 14, 15].

Largely based on the IF97 model, other researchers have developed approximation models for water and steam in order to further improve the computing speed. Åberg [10] fit fifth order polynomials to the IF97 models with spline functions to smooth the phase change transitions. Hofmann et al. [11] implemented linear and quadratic approximation functions for pressure-based sub-regions with interpolation methods for in-between states. Further, some models cover a subset of phase regions, such as the saturated water and steam line functions by Affandi et al. [12] and the incompressible liquid water models in the MBL [7]. In addition, there are other interpolation and table-based methods for reducing computing time and smoothing phase-change transitions. These include spline-based table look-up (SBTL) [16], look-up table interpolation [17], bi-cubic spline interpolation [18], bi-quadratic spline interpolation [19], and tabular Taylor series expansion [20, 21]. However, these methods are data intensive and are often most suitable for computational fluid dynamics and other applications that require a fine discretization of property evaluations, such as a pressurized water reactor in nuclear systems. This is in contrast to thermo-fluid modeling for DH applications, where the scalability from small to large districts is a primary concern. Thus, table-based methods were excluded from Table 1.

For nuclear and power plant applications, there are numerous computational codes available that meet the requirements of fast and accurate two-phase flow modeling for those domains. To evaluate thermodynamic properties, most of these codes store in memory the IAPWS-95 or IF97 models as look-up tables and evaluate properties over an indexed region using either fitting functions (e.g., polynomials, splines) or interpolation methods. Further, they often extend and modify the IAPWS base models to include non-equilibrium thermodynamics. For example, RELAP [22] implements the previously-mentioned SBTL method by Kunick and Kretzschmar [16] with the tabulated IAPWS-95 model. Similarly, TRACE [23] uses a tabulated IAPWS-95 dataset and applies polynomial fits (default) or interpolation, while CATHARE [24] uses the REFPROP Library by NIST, which is similarly based on "high accuracy Helmholtz energy equations of state" [25] (just as the IAPWS-95). ATHLET-SC [26] and APROS [27] implement the IF97 model with table look-up methods. Targeting nuclear and power plant systems, these codes require and provide fine discretization for property evaluations, implementing finite difference, finite volume, and finite element methods. Further, they often aim to simulate failure conditions such as a small break loss-of-coolant accident, which require accurate evaluation of fast transients at extreme temperature/pressure conditions. For these applications, the table-based methods are effective both in terms of accuracy and computational speed, as demonstrated by Zhong et al. [28] in their comparative evaluation between TRACE and RELAP (table-based IAPWS-95) and the IF97 models implemented analytically.

The water and steam medium models reviewed above have been adopted in steam-based simulation studies spanning multiple domains and system boundary scopes. Numerous studies focus on steam plants. For example, Beiron et al. [29] simulated with Modelica waste-fired CHP plants using Modelon's Thermal Power Library [30] (its *Water Polynomial* model uses IF97 as a base). Huang et al. [31] simulated combined cooling, heating and power systems during off-design conditions and adopted the IF97 model. Zhang et al. [32] similarly used the IF97 model while simulating integrated solar combined cycle systems. Several steam plant simulation studies do not declare which medium model they adopted for steam and water thermodynamics, but still ought to be mentioned. These simulation studies include ultra-critical biomass steam power plants [33], new industrial waste heat recovery systems with seasonal thermal storage [34], new waste heat DH systems with CHP [35], and optimization of coal-fired CHP to decouple heat and power modes [36]. In addition to Modelon's Thermal Power Library [30], there are numerous Modelica libraries suitable for steam plants, such as ClaRa+ [37] and ThermoSysPro [38].

Contrary to studies focusing on steam plants, others have focused on DH networks. For example, commercial software packages such as Termis by Schneider Electric [39] can help

with design and planning of steam DH piping networks but does not include plant models. Termis uses the ASME steam tables for property evaluation, and the condensate return temperature from buildings must be explicitly defined by the user for steam systems. In literature, some studies focused on steam piping networks as well. For example, Wang et al. [40] modeled steam piping networks dynamically in Modelica for industrial applications. Similarly, Wang et al. [41] considered drainage loss in steam pipeline network models for recovery purposes, while Jie et al. [42] optimized pressure drop in steam piping networks from environmental perspectives. Among all of these examples, thermodynamic states at source nodes are user-defined inputs (i.e., the plant supply or building condensate return), either via historic measured data or real-time measurements through Supervisory control and data acquisition systems, and the simulations solve for states at sink nodes. Lastly, numerous studies and tools focus on buildings connected to DH networks. While a comprehensive review of these building-level works is out of the scope of this paper, many established simulation codes can simulate buildings fed by steam piping, including EnergyPlus [43].

1.3. Contributions

As exemplified by the literature review, steam system simulation codes and literature to date have focused on one of three system boundaries: (1) the plant, (2) the distribution network, or (3) the building. However, there are increasing demands for complete steam DH simulations. These three scope boundaries as well as the fourth emerging system boundary for complete districts are depicted in Figure 1. It is important to note that literature on modeling and simulation of complete hot water DH systems is abundant [44, 45, 46, 47] but out of the scope of this paper. The primary contribution of this work is to enable simulations of complete steam DH systems that are sufficiently fast and accurate for practical adoption by industry professionals for annual simulations.

While existing simulation codes are effective within their scope boundaries, new simulation challenges arise with the need for complete steam DH simulations. First, complete district simulations (system boundary #4) contains *multiple parallel closed loops* in the thermo-fluid system that grow linearly with the number of buildings N. These thermo-fluid loops can create coupled systems of nonlinear equations. Solving these coupled systems of nonlinear equations require the application of iterative nonlinear solvers, which can be computationally costly. System boundaries 1 through 3 do not have this problem, since they are either open loops (boundary #2) or contain a smaller set of algebraic loops within the plant (boundary #1) or building (boundary #3). High-order building models can have this same challenge when used with implicit ordinary differential equation solvers, but reduced-order building models are frequently used for district-scale analysis to meet computational needs. Second, steam heating systems involve phase changes that typically cross the two-phase wet steam region. With this, discontinuities in the thermodynamic functions at the phase change boundary can cause chattering [18] and at times simulation failure. Further, the IF97 model contains separate

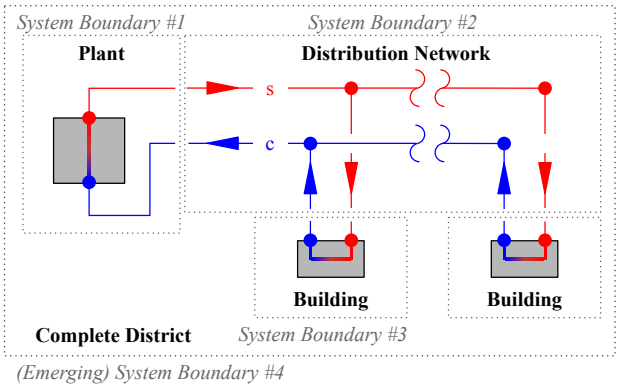

Figure 1: Scope boundaries for steam district heating simulation with steam (s) and condensate (c) connections.

forward and backward equations that are not analytical inverses, i.e., $h(p, T(p, h^*)) \neq h^*$ for some $p, h^* \in \mathfrak{R}$. This can cause serious error accumulation in lengthy calculations [20] and can be an additional source of chattering [48]. Yet on the other hand, the IAPWS-95 model contains only a single set of equations in terms of (ρ, T); thus, costly iterative methods are required to solve thermodynamic properties if other inputs are known, such as (p, T) or (p, h).

To address these gaps and limitations, we propose a new water and steam modeling approach with sufficient accuracy and computing speed for large-scale thermo-fluid system modeling and simulation in practical industry applications. First and foremost, we replace the mathematical formulations for the subcooled liquid region with a numerically efficient model while retaining the commonly-adopted IF97 formulations of thermodynamic properties in the other regions. To our best knowledge, this split medium approach is atypical and has not yet been tested in the context of system simulation of steam heating and industrial processes. Our hypothesis is that by splitting the water/steam medium into different models, we can break the algebraic loops of steam DH systems, therefore improving computing speed with negligible sacrifice to accuracy. Secondly, we also replace commonly-called thermodynamic functions for the superheated vapor region with polynomial approximations in a reduced p-T range. While this reduced range does not apply to all steam systems, its intention is to evaluate the effects of IF97's inconsistent forward-backward equations and high-order mathematical models in the superheated vapor region. When suitable for the intended application, these secondary simplifications may further reduce computing time and numerical challenges for industry practitioners. In addition, we develop several new component, equipment, and system models that allow numerically efficient simulations of DH systems with our novel approach.

1.4. Paper Organization

The rest of this paper is organized as follows. In section 2, we present the models adopted through this work, including our split-medium implementations and several component models. In section 3, we present our approach for evaluating the water

and steam implementation across several scales: at thermodynamic property scale, component scale, and district scale. The results and discussion for each of these three levels of evaluation are then presented in section 4 and section 5, respectively. Lastly, final conclusions are provided in section 6.

2. Modeling Approach

To meet the objective of fast and accurate steam DH modeling for practical applications, we propose new models from mediums to components that can be assembled into complete district energy systems. Component models leverage the novel split-medium approach when phase-change is present (e.g., steam boilers, heat exchanges). It is worth noting that the Modelica Standard Library (MSL) and the MBL decouple balance equations and media model equations; thus the same balance equations and components can adopt various medium models, regardless of whether the media uses (T, p) or (ρ, T) as independent variables, or whether the media is incompressible or compressible. Thus, the various models in subsection 2.1 can be used in components and systems models presented throughout this paper.

2.1. Medium Models

The medium modeling objective is to evaluate the accuracy and computing speed of split-medium models with respect to the standard implementations of IF97 and IAPWS-95. All six regions for water/steam thermodynamics, depicted in Figure 2, are covered by the IF97 and IAPWS-95 formulations. As previously mentioned, the IF97 model is most commonly adopted; as such, it was readily available through the open-source MSL [49] as their *Standard Water* model. The IAPWS-95 model was previously implemented in Modelica by Márquez et al. [50], but their implementation was not compatible with the MSL and therefore could not be used directly. For comparative evaluation, we implemented the IAPWS-95 model in a way that follows the medium definition in the MSL [51]. This new implementation allows us to compare the IAPWS-95 model with the IF97 and our novel split-medium approaches across multiple scales. Our IAPWS-95 implementation was validated with the computer program verification test values given in the standard [8]. For reference, the IAPWS-95 equations and the IF97 equations for the superheated vapor region that we implemented in this work are included in Appendix A and Appendix B, respectively.

Shown in Table 2, our novel split-medium models cover the same regions as the IF97 and IAPWS-95 models, except the supercritical region 6 in two of the three cases, and reduced pressures in regions 1 and 5. First, case *IF97+TDD* pairs the IF97 model with the temperature dependent density water model (TDD) from the MBL. This TDD model assumes an incompressible fluid with, as the name implies, density as a function of temperature. In addition, the TDD model assumes by default a constant value of 4184 J/kg-K for both isobaric c_p and isochoric c_v specific heats, which corresponds to 20°C. Second, case *S+TDD* further replaces the superheated vapor region 5 with the simplified steam model S. Here, S refers to the

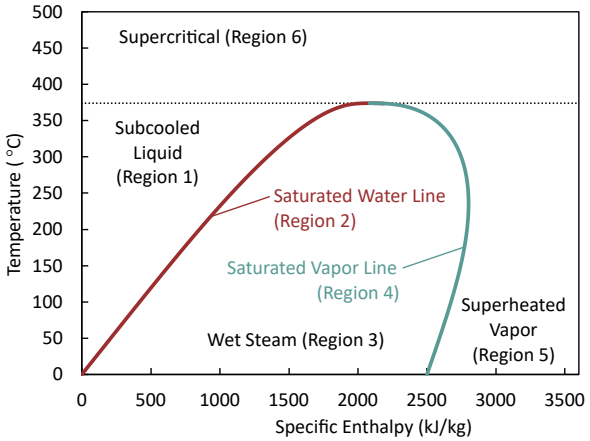

Figure 2: Temperature-enthalpy diagram for water and steam with adopted region definitions.

complete simplified steam formulation, which includes thermodynamic property formulations from the IF97 model with the equations for $h(\cdot)$ and $s(\cdot)$ replaced by approximation functions $\hat{h}(\cdot)$ and $\hat{s}(\cdot)$, which are given in Appendix C. Further, the wet steam region 3 is covered through the balance equations with equilibrium assumptions, as presented in section 2.3.3. Third, case *S+CD* is the same as *S+TDD* except we replace the TDD water model with a constant density water model from the MBL (CD), which is referred as *Water* in the library [7]. This CD model also assumes a constant value for c_p and c_v. Because the TDD and CD models both assume an incompressible liquid, they are less accurate for high pressure conditions. As such, the supercritical region 6 is also excluded from the *S+TDD* and *S+CD* cases, which is typically not required for steam heating applications. These three split medium cases in addition to the two commonly-used cases, referred as IF97 and IAPWS95, are evaluated herein.

2.2. Balance Equations

Several component models can optionally select dynamic or steady state balances for mass and energy dynamics. Since these equations are fundamental to all of the following component models, they are presented here at the onset. Assuming a generic control volume with $\dot{m}_i(\cdot)$ being the mass flow rate through fluid port i and $F \in \mathbb{F}$ being the number of fluid ports, the steady state mass mass balance equation used during time step t is

$$0 = \sum_{i=1}^{F} \dot{m}_i(t). \tag{1}$$

Similarly, the dynamic mass balance is

$$\frac{dm(t)}{dt} = \sum_{i=1}^{F} \dot{m}_i(t). \tag{2}$$

Table 2: Split-medium model implementations by region, with the entire water/steam model covered by two models delineated at the saturated water line. Abbreviations IF97 is the IAPWS IF97 formulation (Appendix B), S is the simplified steam model (Appendix C), TDD is referred as *TemperatureDependentDensity* in the MBL [7], and CD is referred as *Water* in the MBL [7]

Region	*Split-medium approaches*		
	IF97+TDD	*S+TDD*	*S+CD*
		Model 1	
1	TDD	TDD	CD
		Model 2	
2	IF97	IF97	IF97
3	IF97	Control volume[1]	Control volume[1]
4	IF97	IF97	IF97
5	IF97	IF97+$\hat{h}(\cdot)$+$\hat{s}(\cdot)$ [2]	IF97+$\hat{h}(\cdot)$+$\hat{s}(\cdot)$ [2]
6	IF97	N/A	N/A

[1] The control volume is presented in section 2.3.3.
[2] Approximation equations for the enthalpy (Equation C.5) and entropy (Equation C.8) are given in Appendix C.

The steady state energy balance is

$$0 = \sum_{i=1}^{F} \dot{m}_i(t) h_i(t) + \dot{Q}(t), \tag{3}$$

where $h_i(\cdot)$ is the specific enthalpy for fluid connector i and $\dot{Q}(\cdot)$ is the heat flow rate entering the volume. Meanwhile, the dynamic energy balance is

$$\frac{dU(t)}{dt} = \sum_{i=1}^{F} \dot{m}_i(t) h_i(t) + \dot{Q}(t), \tag{4}$$

where $U(\cdot)$ is the energy stored in the volume. Because a steady state energy balance coupled with a dynamic mass balance can lead to inconsistent equations, all models require the energy and mass balances to be the same type. For the specific evaluation models included in this paper, the mass and energy balances assigned to each component model as well as the initial conditions are included in section 3.

2.3. Component Models

This section presents component models that are fundamental to this work. While a complete description of all models available for steam DH systems is out of the scope, interested readers can find more information in the open-access MBL [7] and MSL. For example, the check valve, feedwater tank, the PID control block, and various thermodynamic sensors (see Figure 7) are publicly available in the MBL, while the table input used for the building heat load profile as well as the various mathematical operation blocks (see Figure 8) can be found in the MSL. All component models that involve water/steam phase change and the two-phase region were implemented specifically for the split-medium approach with this work; however, the fundamental mathematics apply for both the split medium and traditional single medium approaches. Lastly, some of these components are existing models in the MBL (pump, pressure drop), while the control volume, boiler, and steam trap are new.

2.3.1. Pump

In steam DH systems, pumps supply feedwater at the plant and at times return condensate to the plant from buildings. Because pumps notably contribute to the fluid dynamics and electricity consumption, we include the model details here. We implement the pump model from the MBL that uses performance curves to compute pressure rise Δp, electrical power draw P, and efficiency η as functions of volumetric flow rate $\dot{V}$ and rotational speed r. The pump model is consistent with the affinity laws $\Delta p \propto r^2$ and $\dot{V} \propto r$. To ensure that solutions to the differential algebraic system of equations posed by the thermo-fluid model can be computed robustly and efficiently by Newton-based solvers, the pump is formulated in such a way that the resulting equations of the fluid flow network has a unique solution in each operable region and is differentiable in all inputs. While complete details for the pump formulation are available in [52], the fundamental formulation when the pump operates far from the origin is as follows. Let $\delta = 0.05$ be a small number that is below the typical normalized pump speed and $\mathcal{S}_n^{'} = \{(\dot{V}_i, \Delta p_i)\}_{i=1}^{n}$ be the user-supplied performance data at full speed $r = 1$, with $\dot{V}_i \geq 0$ and $\Delta p_i \geq 0$ for all $i \in \{1, \ldots, n\}$. Here, n represents the total number of operating points. For conditions $r > \delta$ (i.e., far from the origin), the affinity laws are satisfied while the maximum volumetric flow rate $\dot{V}_{max}$ and maximum pressure change Δp_{max} are linearly extrapolated as

$$\dot{V}_{max} = \dot{V}_n - \frac{\dot{V}_n - \dot{V}_{n-1}}{\Delta p_n - \Delta p_{n-1}} \Delta p_n \quad \text{and} \tag{5}$$

$$\Delta p_{max} = \Delta p_1 - \frac{\Delta p_2 - \Delta p_1}{\dot{V}_2 - \dot{V}_1} \dot{V}_1. \tag{6}$$

The pump performance curve for $r > \delta$ is defined as

$$\Delta p^{+}(r, \dot{V}) = -\Delta \hat{p}(\dot{V}) + r^2 h\left(\frac{\dot{V}}{r}, \mathcal{S}_n^{'}\right), \tag{7}$$

with the curve end points represented by $\Delta p^{+}(1, \dot{V}_{max}) = 0$ and $\Delta p^{+}(1, 0) = \Delta p_{max}$, while $h(\cdot, \mathcal{S}_n^{'})$ is a cubic Hermite spline that maps $\dot{V}$ to Δp, and $\Delta \hat{p}(\dot{V})$ approximate the flow resistance of the pump, for reasons of numerical robustness, by a linear function as

$$\Delta \hat{p}(\dot{V}) = \dot{V} \frac{\Delta p_{max}}{\dot{V}_{max}} \frac{\delta^2}{10}. \tag{8}$$

In addition to conditions $r > \delta$, Wetter [52] also defines formulations for near origin ($r < \delta/2$) and composite ($r \in [\delta/2, \delta]$) conditions to complete the pump model. In this case study, we assume a constant hydraulic efficiency $\eta_h = 70\%$ and a constant electric motor efficiency $\eta_m = 70\%$. Total efficiency η is then

$$\eta = \eta_h \eta_m, \tag{9}$$

and the electrical power draw is computed as

$$P = \frac{W_{fl}}{\eta}, \tag{10}$$

where W_{fl} is the flow work defined per the first law as

$$W_{fl} = |\dot{V}\Delta p|. \tag{11}$$

In this model, $\dot{V}$ is calculated from $\dot{m}$ with the density defined at the inlet port ρ_1 as $\dot{V} = \dot{m}/\rho_1$.

2.3.2. Pressure Drop

To account for pressure drop in pipes and other components, we use a flow resistance model from the MBL that has a fixed flow coefficient, named *Pressure Drop* in the library. To decouple the energy and mass balance equations, pressure drop Δp is a function of the mass flow rate, rather than the volumetric flow rate. This model computes Δp as

$$\Delta p = \text{sign}(\dot{m})\left(\frac{\dot{m}}{k}\right)^2, \tag{12}$$

where $\dot{m}$ is the mass flow rate and k is a constant flow coefficient calculated from the nominal mass flow rate $\dot{m}_0$ and nominal pressure drop Δp_0 as

$$k = \frac{\dot{m}_0}{\sqrt{\Delta p_0}}. \tag{13}$$

With the inverse $\dot{m} = k\sqrt{\Delta p}$ also implemented in the library, this model replaces the square root with a differentiable function with a finite slope for conditions $\dot{m} < \delta_t \dot{m}_0$, where δ_t is the fractional mass flow rate where the transition to turbulent flow occurs (set to 0.3 by default but adjustable by the user). Further information about the regularization near the origin and the basic flow models is available in the MBL [7].

2.3.3. Control Volume

The new control volume model can represent either evaporation or condensation processes with the liquid and vapor subcomponents in equilibrium. This model is designed to assign each of the two medium formulations of the split-medium approach (Table 2) at the inlet and outlet ports. For an evaporation process, the subcooled liquid water medium is assigned to the inlet, while the composite water/steam medium is assigned to the outlet. The opposite is true for the condensation process. The mathematical formulation for the evaporation process is consistent with the existing drum boiler implemented in the MSL [53]. Both the evaporation and condensation control volumes have the following assumptions:

1. The fluid within the volume is wet steam (region 3);
2. Liquid and vapor subcomponents are at equilibrium; and
3. Fluid is discharged from the volume as either saturated liquid or saturated vapor.

It should be noted that these assumptions restrict the possible use cases (e.g., the volume cannot model superheated or subcooled fluids). An additional limitation is that any sensible heat losses/gains downstream of the control volume must be included in a separate component. While this additional step can increase model development time, from our experience, the time saved by avoiding common numerical challenges greatly outweighs the former inconvenience.

The fundamental equations are as follows. Let subscripts 1 and 2 represent the inlet and outlet ports, respectively. The fluid mass m in the volume is calculated as

$$m = \rho_1 V_1 + \rho_2 V_2, \tag{14}$$

where ρ is density and V is volume.

The total internal energy U is

$$U = \rho_1 V_1 h_1 + \rho_2 V_2 h_2 - pV, \tag{15}$$

where h is specific enthalpy, p is pressure, and $V = V_1 + V_2$ is the total volume of the fluid.

More specifically, since the volume contains a saturated mixture, h_1 and h_2 are the specific enthalpies of saturated vapor and saturated liquid for a condensation process. These assignments are reversed for an evaporation process. As a saturated mixture at equilibrium, the vapor quality χ is defined as

$$\chi = \begin{cases} m_1/m, & \text{if condensation,} \\ m_2/m, & \text{if evaporation,} \end{cases} \tag{16}$$

which is used to calculate thermodynamic properties of the wet steam two-phase mixture. For example, the specific enthalpy of wet steam is

$$h = \frac{m_1 h_1 + m_2 h_2}{m}. \tag{17}$$

As previously mentioned, the control volume is configured to allow both steady state and dynamic mass and energy balances. The steady mass, dynamic mass, and dynamic energy balances are consistent with Equation 1, Equation 2, and Equation 4, respectively, with $F = 2$. However, the steady energy balance for a wet steam control volume at equilibrium has an additional constraint. Because the discharging fluid is constrained at pressure $p = p_{sat}$ with $T = T_{sat}(p_{sat})$ and saturated enthalpy $h = h_2(p_{sat})$, where subscript *sat* is the saturated state, if the mass and energy balances are steady, then prescribing the heat flow into the volume $\dot{Q}$ over-constrains the problem. Thus, Equation 3 is not included in this model; instead, $\dot{Q}$ is directly proportional to the mass flow rate and is calculated as

$$\dot{Q} = \dot{m}_1 h_{fg}, \tag{18}$$

where $h_{fg} = h_2 - h_1$ is the enthalpy of vaporization. Thus, when used as a steady state model, this heat must be removed from the system in which this volume is used.

2.3.4. Boiler

Figure 3 shows the schematic model view of the boiler that discharges saturated steam and has an efficiency curve defined by a polynomial. The rate of heat transferred to the water

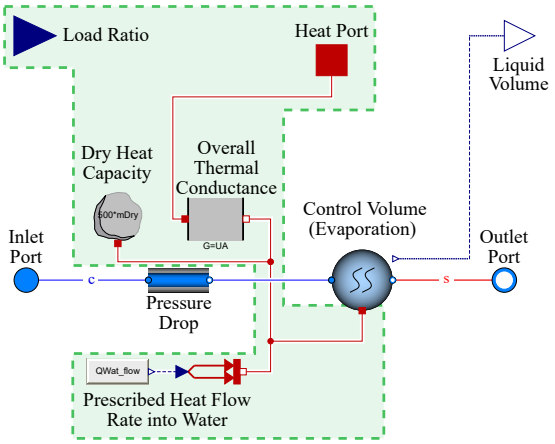

Figure 3: Modelica diagram for the boiler with an efficiency curve defined by a polynomial. Components in the green shaded region (including the heat port for the control volume, but not the volume itself) are conditionally removed if the boiler is configured with steady state mass and energy balances.

medium $\dot{Q}$ is

$$\dot{Q} = y\,\dot{Q}_0\,\frac{\eta}{\eta_0}, \tag{19}$$

where $y \in [0, 1]$ is the load ratio, $\dot{Q}_0$ is the nominal heat capacity, η is the total efficiency at the current operating point, and η_0 is the total efficiency at $y = 1$ and boiler output temperature $T = T_0$, where T_0 is the nominal temperature. With efficiency $\eta = \dot{Q}/\dot{Q}_f$ and $\dot{Q}_f$ representing the rate of heat released by the fuel combustion, the three polynomial options to compute η are

$$\eta = a_1, \tag{20}$$

$$\eta = a_1 + a_2 y + a_3 y^2 + \ldots + a_n y^{n-1}, \quad \text{and} \tag{21}$$

$$\eta = a_1 + a_2 y + a_3 y^2 + (a_4 + a_5 y + a_6 y^2) T, \tag{22}$$

where a_1 through a_n are regression coefficients.

Similar to the control volume, the boiler model can have steady or dynamic mass and energy balances. If the boiler is configured in steady state, then several components (highlighted in green in Figure 3) are conditionally removed to maintain a consistent set of equations. The reason is the same as the control volume, where $\dot{Q} = f(\dot{m})$; therefore, if the mass and energy balances are steady, then prescribing the heat flow into the fluid over-constrains the problem, and thus they are removed. Conversely, dynamic balances enable the heat flow rate into the control volume to be calculated based on the heat transfer from the fuel and through the boiler's enclosure with the external environment.

2.3.5. Steam Trap

A required component of steam heating systems, steam traps effectively ensure that only liquid condensate leaves components (e.g., steam heat exchanger), while any flashed steam is returned to a liquid state before discharge. This prevents the loss of steam while protecting pipes for water from damage by hot and high pressure steam vapor. In this model, we assume steady state mass and energy balances. The steam trap represents an isenthalpic thermodynamic process that transforms liquid water from an upstream high pressure (state 1) to atmospheric pressure (state 2a), followed by an isobaric condensation process to return flashed steam to a saturated liquid (state 2). The heat loss in the trap $\dot{Q}_l$ is

$$\dot{Q}_l = \dot{m}(h_{2a} - h_2), \tag{23}$$

where $\dot{m}$ is the steady state mass flow rate, and h_{2a} and h_2 are the specific enthalpies at states 2a and 2, respectively.

3. Evaluation Approach

To evaluate the accuracy and computing speed across multiple spatial scales, Modelica models are developed at thermodynamic property scale (simple function evaluations), component scale (a control volume), and district scale (complete heating districts of several sizes). Several medium model implementations are used within the component models for the component and district scale evaluations. Two cases involve the IF97 model, IF97(MBL) and IF97(MSL); one case involves the IAPWS-95 model, IAPWS95(MSL); and three cases use our split-medium approach, IF97+TDD, S+TDD, and S+CD. With the two IF97 cases, models from two separate libraries are evaluated: the MBL and MSL, while the IAPWS95 model is only evaluated with the MSL. Even though the models from both the MBL and MSL libraries can be applied for steam DH applications, their original design intentions differ, and correspondingly, they are based on different assumptions. The IF97(MBL) and IAPWS95(MSL) cases are only used in the component-scale evaluation. The remaining four cases are common to both. Further details regarding the model setup for each simulation case are provided in the following sections.

Several new component and system models for DH modeling were developed for these case studies, as presented in section 2. These models are in the process of being refined and open-source released in the MBL. Beyond newly developed models, all components used are existing in the MSL v3.2.3 and MBL v7.0.0.

3.1. Thermodynamic Property Scale

The accuracy and computing speed of several thermodynamic property functions are evaluated with respect to the IF97 and IAPWS-95 models. These include the subcooled liquid water models from the MBL (CD and TDD) as well as the superheated vapor approximation functions for specific enthalpy (Equation C.5) and entropy (Equation C.8), which are integrated into model S. The objective was to evaluate solely the thermodynamic properties separate from higher-level effects from components, equipment, and systems. For accuracy, we calculated the absolute and percent differences between the numerically improved functions (CD, TDD, S, and IF97) and the IAPWS95 model across their respective p-T ranges.

To evaluate computing speed, we also present the computing time for thermodynamic property evaluations using different formulations – IF97, IAPWS95, CD, TDD, S – and different independent variables – (p, T), (p, h), and (ρ, T). As previously mentioned, the IF97 and the numerically efficient liquid water

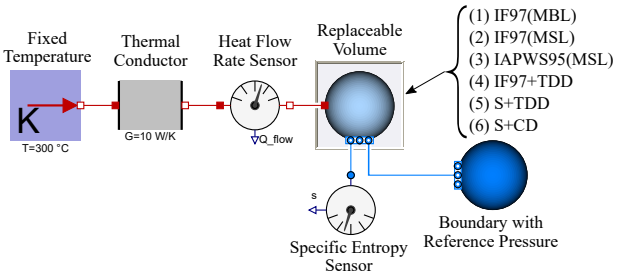

Figure 4: Diagram of Modelica model for control volume evaluations.

and steam vapor models contain both forward and backward equations for various properties, while the IAPWS95 formulation strictly has independent variables of (ρ, T). Thus, the selection of independent variables can significantly impact computing time.

3.2. Component Scale

Because of the discontinuities at the phase-change barrier, numerical solvers have shown to experience difficulties solving thermo-fluid problems with two-phase flow. Chattering is one example of a well-known issue that has been demonstrated previously with a Modelica-based simulation of a boiler pipe model featuring the IF97 medium [18]. For this case, we use a control volume (section 2.3.3) to evaluate the performance of the split-medium implementations compared to the IF97 and IAPWS95 models with control volume models in the MSL and MBL. This component-scale experiment was selected to isolate some of the common numerical challenges of thermo-fluid system modeling involving phase change that may not appear at smaller scales while being harder to diagnose at larger scales.

Shown in Figure 4, the Modelica-based evaluation features a water control volume of 0.1 m^3 that is exposed to a constant temperature boundary of 300°C via a thermal conductor with a constant thermal conductance of 10 W/K. The volume is configured with dynamic energy and mass balance equations, and the initial condition $p(t_0)$ is set at the reference pressure of 200 kPa due to the connection with the Boundary component. The control volume is replaceable in order to allow six different mediums to be simulated with the same experimental setup.

In the component-scale evaluation, three baseline cases are included – IF97(MBL), IF97(MSL), and IAPWS95(MSL) – and three cases from Table 2 are included – IF97+TDD, S+TDD, and S+CD. First, the MBL case with the IF97 model – IF97(MBL) – includes the control volume designed for single-phase fluid, referred as *Mixing Volume* in the MBL Fluid package. Second, the MSL cases with the IF97 and IAPWS-95 models – IF97(MSL) and IAPWS95(MSL) – implement a two-phase equilibrium boiler model [53], referred as *Equilibrium Drum Boiler* in the MSL Fluid package. This model was designed for water-steam phase change and is mathematically equivalent to the control volume presented in section 2.3.3. The remaining three split-medium cases all use the new control volume. The other model components in Figure 3 (e.g., thermal conductor, sensors, pressure-temperature boundary) are freely available in the MBL. For accuracy, we evaluated the Root Mean Square Error (RMSE) and Coefficient of Variation of the Root Mean Square Error (CVRMSE) using

$$RMSE = \sqrt{\frac{\sum (y_i - \hat{y}_i)^2}{N}} \quad \text{and} \tag{24}$$

$$CVRMSE = \frac{RMSE}{\bar{y}}, \tag{25}$$

where y_i is the individual reference data generated by the IF97 model, $\hat{y}_i$ is the corresponding evaluation data predicted by the new model, $\bar{y}$ is the mean of the reference dataset, and N is the total number of data points.

3.3. District Scale

The objective of the district scale evaluation was to assess the accuracy and numerical performance of the new split-medium approach in a typical DH system design across districts of several sizes. An overarching description of the selected system is presented next, followed by the Modelica implementation.

3.3.1. System Description

Figure 5 depicts the schematic diagram for the DH evaluation. This DH system is broken into three subsystems: a central plant, the distribution network, and building end users. The central plant features a feedwater tank, feedwater pump, and a single steam boiler. Saturated steam is discharged from the boiler at 300 kPa. The fuel load ratio for the boiler is controlled to maintain the boiler discharge pressure, while the feedwater pump speed is controlled to maintain the liquid water level in the boiler. While there are several mechanical and control designs seen in central plants [54], this configuration was selected because it represents real-world control dynamics while representing one of the more simple designs. For the distribution network, we assume there are no mass nor energy losses in the steam supply pipe, while the condensate return pipes have fixed pressure drops without any heat transfer. Although heat and mass losses in steam supply pipes are not negligible in real-world systems, there is no Modelica model available for a saturated steam pipe with drip-leg, to our knowledge. While out of the scope of work for this paper, we are currently developing a model for this purpose that will be made public in the future, which features a steam pipe (heat losses, mass losses, flow resistance, transport delays) with a drip-leg (condensate recollected). Lastly, the buildings contain a steam heat exchanger (modeled as a condensation control volume), a steam trap, and a condensate return pump. For demonstration purposes, we apply the same variable heating load profile to all buildings, which can be seen in Figure 8 of section 4. The mass and energy balances for all components in the district scale simulation as well as the initial conditions are summarized in Table 3.

3.3.2. Modelica Implementation

To evaluate the steam medium implementation across a variety of district sizes, a vector-style DH system model was developed in Modelica (Figure 6). This top-level Modelica diagram has a clear one-to-one relationship with the subsystems

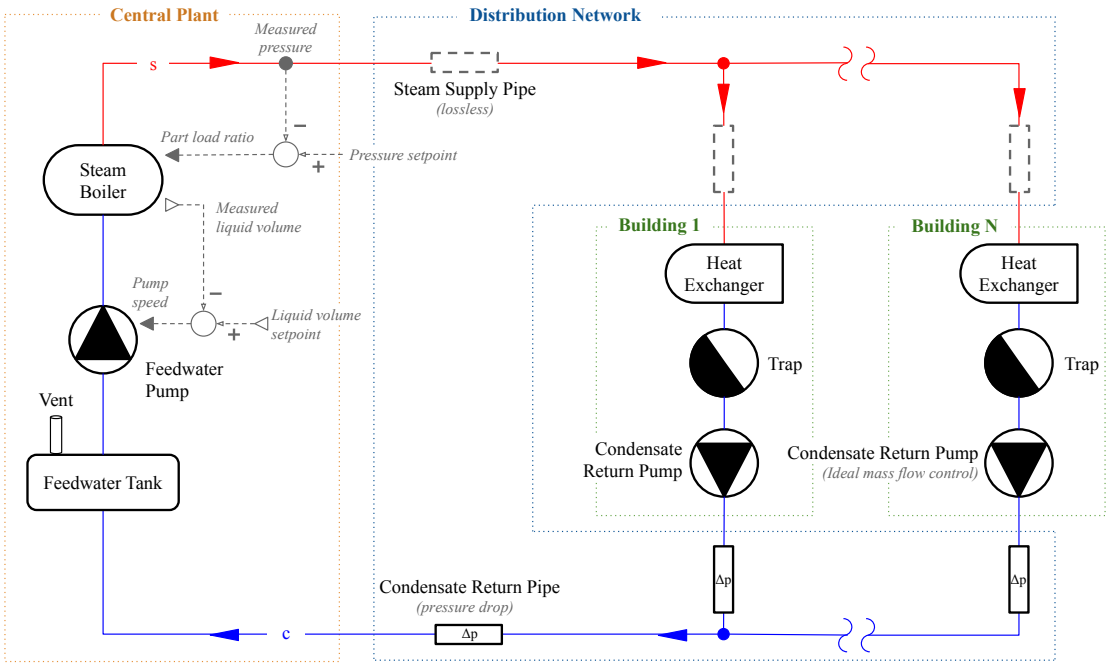

Figure 5: Schematic diagram of DH steam loop with a central plant, distribution network, and N number of interconnected buildings.

Table 3: Initial conditions as well as mass and energy balances for the district scale evaluation model, where N is the total number of buildings and n_i is the number of buildings connected to pipe segment i.

Subsystem	*Component*	*Initial Conditions*			*Balance*
		p (Pa)	T (°C)	$\dot{m}$ (kg/s)	*Equations*
Plant	Feedwater tank	101325	20	$(7.38 \times 10^{-3})N$	Dynamic
	Feedwater pump	101325	20	$(7.38 \times 10^{-3})N$	Dynamic
	Check valve	101325	20	$(7.38 \times 10^{-3})N$	Steady
	Boiler	300000	133.5	$(7.38 \times 10^{-3})N$	Dynamic
Distribution network	Supply pipes (lossless)	300000	133.5	$(7.38 \times 10^{-3})n_i$	Steady
	Return pipes (pressure drop)	101325	100	$(7.38 \times 10^{-3})n_i$	Steady
Building	Heat exchanger	300000	133.5	7.38×10^{-3}	Steady
	Steam trap	300000	133.5	7.38×10^{-3}	Steady
	Condensate return pump	101325	100	7.38×10^{-3}	Dynamic

depicted in Figure 5. A parameter N representing the total number of buildings can be adjusted to represent districts of multiple sizes. The boiler's rated heating capacity is scaled by N in order to adjust for the variable heating capacity of the entire system. This DH system is simulated for two days.

The plant model diagram is shown in Figure 7. In the central plant, the feedwater pump and boiler both have dynamic energy and mass balances, and PI controllers are used to maintain the water level and pressure setpoints. A check valve was also included in the central plant model in order to prevent unintended reverse flow. Both the thermal conductance and heat capacity of the boiler drum metal and insulation are included in the model. The boiler is assumed to have constant efficiency with $\eta = 90\%$.

The building model diagram is shown in Figure 8. Through the *Tabulated Heating Load* data reader, the generic variable heat flow rate $\dot{Q}$ is input directly. A condensate return pump

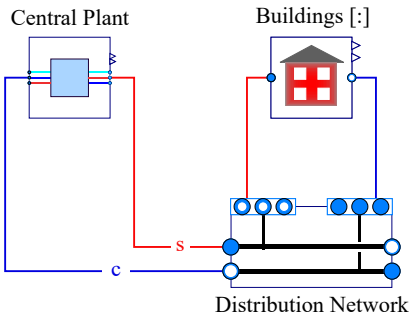

Figure 6: Top level diagram of Modelica model for the DH system.

prescribes the mass flow rate, set to $\dot{m} = \dot{Q}/(h_1 - h_2)$, where h_1 and h_2 are the measured inflowing and outflowing specific en-

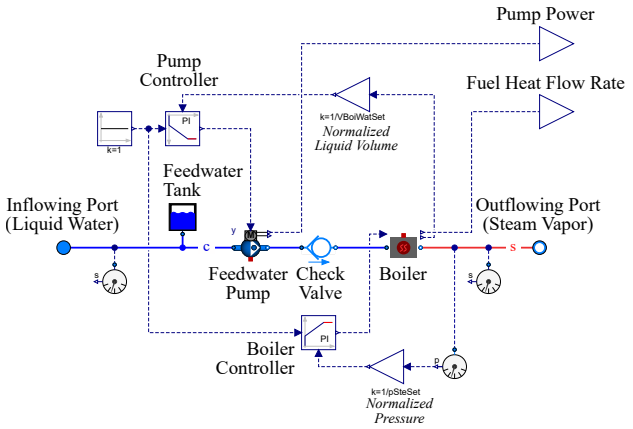

Figure 7: Diagram of Modelica model for the central plant.

thalpy values, respectively. The *Heat Exchanger Volume* model is an instance of the control volume (subsubsection 2.3.3), configured as a condensation process with steady state mass and energy balances. Lastly, the *Steam Trap* represents a steady isenthalpic process where liquid condensate is discharged at atmospheric pressure, as described in section 2.

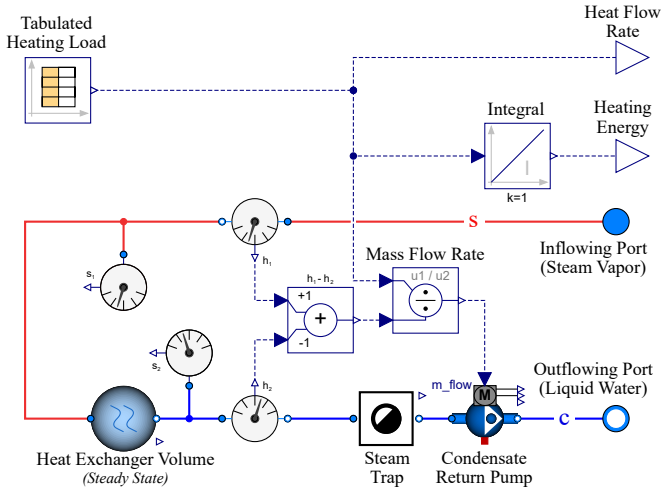

Figure 8: Diagram of Modelica model for the interconnected building.

Four medium model configurations were included in this evaluation: IF97(MSL), S+CD, S+TDD, and IF97+TDD. We were unable to resolve the numerical challenges of the IAPWS95 model for the complete steam DH simulations, particularly for large district sizes. Thus, this model was not included in the district scale evaluation. These challenges are primarily due to (1) the lack of backward equations to represent thermodynamic functions in terms of variables other than (ρ, T) and (2) the highly nonlinear thermodynamic property functions that require precise starting values with implicit solvers. However, this is not to say that the IAPWS95 model cannot be used for complete DH simulations, but only that the numerical hurdles are significantly greater than the other implementations.

3.4. Simulation Settings

All simulations ran in Dymola 2021 on a Windows 10 workstation with a Intel® Xeon® 3.60GHz CPU and 32.0GB of RAM. The DASSL solver was selected for all case studies, after preliminary tests demonstrated its lower computing time compared to other numerical solvers. The simulation tolerance was set to 10^{-6} for all cases. For the fast thermodynamic and component scale evaluations, computing times presented are average values across 10 repeated simulation runs.

4. Results

This section presents the results from simulations across the three scales: thermodynamic properties, component, and district scales. First the accuracy of the model will be presented, followed by the computing speed.

4.1. Thermodynamic Property Scale

Following the methodology prescribed in subsection 3.1, the results for model accuracy and computing speed at the thermodynamic property scale are evaluated. Because IAPWS95 and IF97 have previously been evaluated over their entire p-T range [8, 9], these results focus on the numerically efficient water models (CD, TDD) in the subcooled liquid region 1 and the simplified steam model (S) with polynomial approximations for commonly called functions in the superheated vapor region 5.

4.1.1. Accuracy

For the subcooled liquid water region, the accuracy of the CD and TDD water models are evaluated with respect to IF97 and IAPWS95 at several sub-critical pressure states. The results for 0.1 MPa, 2 MPa, and 4 MPa are shown in Figure 9. The IF97 model produces the highest accuracy relative to IAPWS95, as expected, with relative differences ranging from 3.13×10^{-4} kJ/kg-K (0.140%) for s to -5.18×10^{-3} kJ/kg-K (−0.109%) for c_p for pressures 0.1 to 4 MPa. Because the functions for h, s, and c_p are the same for CD and TDD models, they produced the same results. Errors in the h and s calculations were generally low, with the highest differences relative to IAPWS95 for both CD and TDD cases being −4.06 kJ/kg (−7.18%) and -5.99×10^{-2} kJ/kg-K (−2.24%), respectively. Calculating c_p with both CD and TDD models produces the largest difference relative to IAPWS95 of −0.560 kJ/kg-K (−11.8%), which occurs near the saturated liquid line at 4 MPa. Lastly for ρ, the TDD case produced better accuracy than the CD case, as expected. The largest errors for the CD and TDD cases also occurred near the saturated liquid line at 4 MPa, with differences relative to IAPWS95 of 17.8×10^5 kg/m^3 (21.8%) and 4.42×10^4 kg/m^3 (5.41%), respectively. Based on these results, we recommend the CD water model to be used in its original design range indicated in Table 2. The TDD model is suitable for a larger range of p-T conditions compared to CD, but this is still a subset of the IF97 range as currently designed.

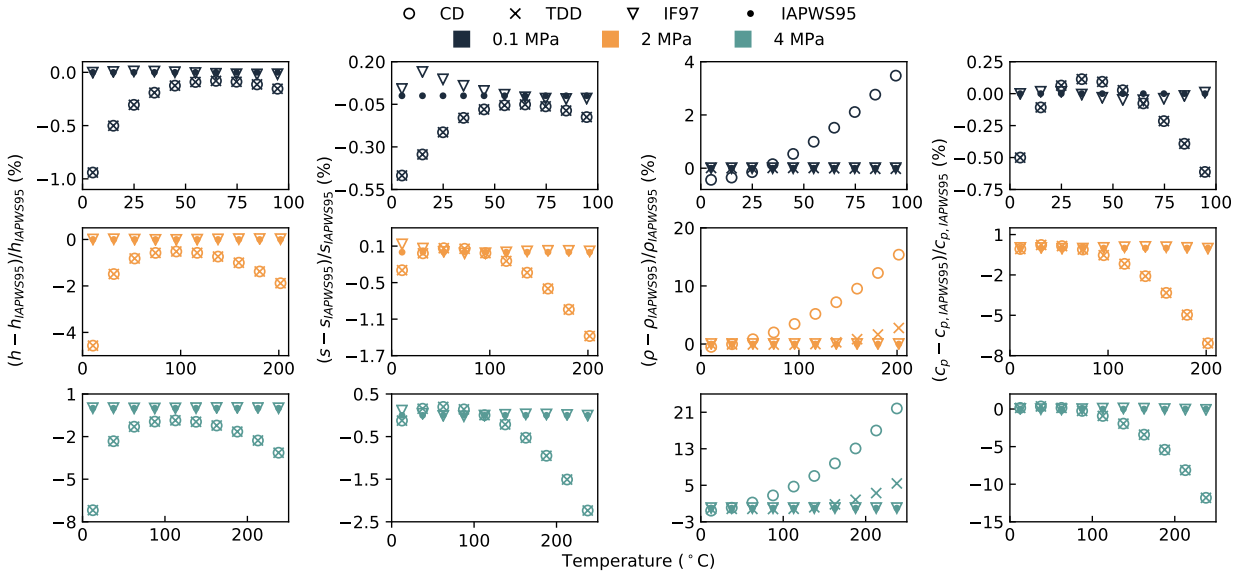

Figure 9: Percent difference of specific enthlapy h, specific entropy s, density ρ, and isobaric specific heat c_p with respect to IAPWS95 values over the range of subcooled temperatures in region 1.

For the new polynomial approximations in the superheated vapor regions (model S), property evaluations for specific enthalpy and entropy produced acceptable accuracy across the entire reduced p-T range. Figure 10 presents the percent differences in h and s calculations for both S and IF97 models relative to IAPWS95. For h, the largest difference between S and IAPWS95 models was −2.42 kJ/kg (−0.090%), which occurred near the saturated vapor line at low p conditions. The reason for this is that the nonlinearities in $h(p,T)$ are higher along the saturated vapor line than other regions. For s, the largest difference between S and IAPWS95 was 0.0470 kJ/kg-K (0.691%), which occurred at high pressure-temperature conditions. The shape of the residuals indicate that the errors are relatively consistent with respect to temperature, but the quadratic fit in pressure underestimates s slightly in the middle of the range while it overestimates s at the high and low limits. Based on these results, the polynomial approximations in model S produce sufficient accuracy in the reduced p-T range. This reduced range is suitable for many steam DH applications, but not all. For steam vapor applications involving higher pressure and temperature states, the IF97 model can still be used with our split-medium approach.

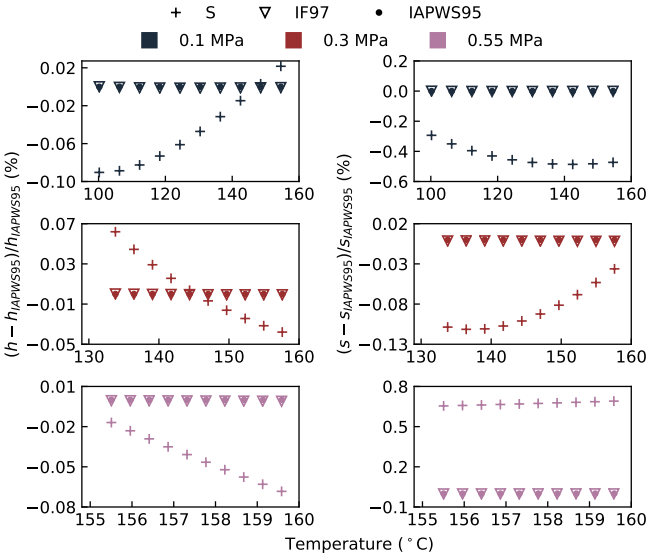

Figure 10: Percent difference of specific enthlapy h and specific entropy s with respect to IAPWS95 values over a range of superheated temperatures.

4.1.2. Computing Speed

Table 4 presents the computing speed results for thermodynamic property evaluations in the subcooled liquid Region 1, where h, s, ρ, and c_p are evaluated over the p-T range shown in Figure 9. The IAPWS95 calculations were significantly slower than all other models, with time savings achieved from 79-92% with IF97, TDD, and CD models. With inputs of (p,T), the TDD and CD models were 24% faster than IF97, while they were both 12% faster with inputs (p,h). With inputs of (ρ,T), the IAPWS95 computing times were 25% and 54% faster than IAPWS95 with inputs of (p,T) and (p,h), respectively. This result follows expectations, since inputs of (ρ,T) induce no nonlinear systems of equations for IAPWS95, while (p,T) and (p,h) induce one nonlinear system with 1 and 2 iteration variables, respectively. However, even when the IAPWS95's design independent variables (ρ,T) are used, IF97 was still significantly faster than IAPWS95 (79% time savings).

Further, we evaluated the computing speed for individual thermodynamic property functions $\hat{h}(p,T)$ (Equation C.5) and $\hat{s}(p,T)$ (Equation C.8) and their backward functions with respect to those from the IF97 and IAPWS95 formulations. The results in Table 5 show that the new polynomial approximations

Table 4: Computing times for thermodynamic property evaluations in subcooled liquid region 1 with time savings evaluated with respect to IAPWS95. Results are averages over 10 simulation runs.

Medium Model	*Input Variables*	*Computing Time (s)*	*Time Savings (%)*
IAPWS95	(p,T)	0.101	–
IF97		0.017	84
TDD		0.013	87
CD		0.013	87
IAPWS95	(p,h)	0.166	–
IF97		0.015	91
TDD		0.013	92
CD		0.013	92
IAPWS95	(ρ,T)	0.076	–
IF97		0.016	79
TDD		N/A[1]	N/A[1]
CD		N/A[1]	N/A[1]

[1] Properties cannot be calculated from (ρ,T) for an incompressible fluid.

Table 5: Computing times for thermodynamic property evaluations in superheated vapor region 5 with time savings evaluated with respect to IAPWS95. Results are averages over 10 simulation runs.

Medium Model	*Equation*	*Computing Time (s)*	*Time Savings (%)*
IAPWS95	$h(p,T)$, A.9	0.100	–
IF97	$h(p,T)$, B.4	0.017	83
S	$\hat{h}(p,T)$, C.5	0.014	86
IAPWS95	$s(p,T)$, A.10	0.101	–
IF97	$s(p,T)$, B.7	0.017	83
S	$\hat{s}(p,T)$, C.8	0.014	86

and the IF97 formulations reduce the computing time by 83%-86% relative to IAPWS95. Relative to IF97, $\hat{h}(p,T)$ and $\hat{s}(p,T)$ were 17% and 14% faster, respectively. Even for these simple thermodynamic property evaluations, the coupled systems of nonlinear equations differed between the IAPWS95, IF97, and S model cases. Both the IAPWS95 and IF97 models produced a nonlinear system of equations that contains a single time-varying variable, while the S formulations did not have any nonlinear systems. In addition, the IAPWS95 model produced a numerical Jacobian, which can be computationally expensive compared to symbolic processing. These factors in the problem formulation can partially explain the computing time results. While the approximation functions $\hat{h}$ and $\hat{s}$ produced savings in computing time at the thermodynamic property scale, the savings are often compounded for larger thermo-fluid system models that involve nonlinear systems of equations. This will be evaluated with the district scale models. However, the computing time savings and calculation accuracies demonstrate how fundamental improvements in steam property modeling can be achieved through function replacement.

4.2. Component Scale

Following the methodology prescribed in subsection 3.2, the results for model accuracy and computing speed at the component scale evaluation are as follows.

4.2.1. Accuracy

Figure 11 depicts the temperature, density, and mass results of the control volume evaluation cases for the model shown in Figure 4. In this simulation, the control volume fluid is heated via a temperature boundary that is at 300°C. With the IF97(MBL) case, undesirable erratic behavior is clear. At initialization, the liquid in the volume is at 40°C. For the first 28 minutes, the temperature gradually increases. However, when water starts to boil, the fluid temperature oscillates between the saturation temperature and the boundary temperature of 300°C. Mass and density are also oscillating in the IF97(MBL) case, as the fluid switches back and forth between one-phase (liquid or vapor) and two-phase states (liquid-vapor mixture). The volume in the MBL case was designed for single phase fluid (air, water, etc.), and functions correctly in those instances. However, it exhibits chattering at phase change when used with the two-phase IF97 medium and the numerical solver DASSL. It is important to note that the MBL behavior seen here is a numerical problem, not a physics problem. Indeed, this numerical problem can be avoided if an *explicit, fixed-time step* method is employed (i.e., Euler) rather than an *implicit, variable-time step* method (i.e., DASSL). With Euler, the IF97(MBL) case performs physically correct and avoids the numerical chattering issue. Further, the IF97(MBL) volume can simulate not only a saturated fluid, but supercooled and superheated fluids as well, which may be of interest for some use cases. However, implicit, variable-time step methods are often used for large thermo-fluid system simulations because of their ability to deal with stiff systems. Thus, the Euler results were excluded from this paper.

The later five cases – IAPWS95(MSL), IF97(MSL), IF97+TDD, S+TDD, and S+CD – perform with the correct physics. Because the MSL and new control volumes were designed for boiling processes with the fluid at a *saturated* state, each of these three cases initialize at the saturation temperature. Throughout the constant pressure boiling process, the liquid volume gradually decreases as more of the water is converted from liquid into vapor, while the temperature of the fluid is held constant. With the simulation entirely within the wet steam region 3, the density of liquid water and steam vapor are similarly maintained.

With the split-medium implementations, some minor accuracy errors are introduced. Since this work targets normal operating conditions, the RMSE and CVRMSE are presented in Table 6 for control volumes with liquid-to-vapor ratios within the ratio of 1 to 9 which are common in real operations. Calculation errors between IF97(MSL) and IAPWS95(MSL) were negligible to none, as expected. Relative to the IAPWS95(MSL) case, the IF97+TDD and S+TDD cases generally produced lower errors than the S+CD case. This was to be expected, because the liquid water with constant density is being applied outside

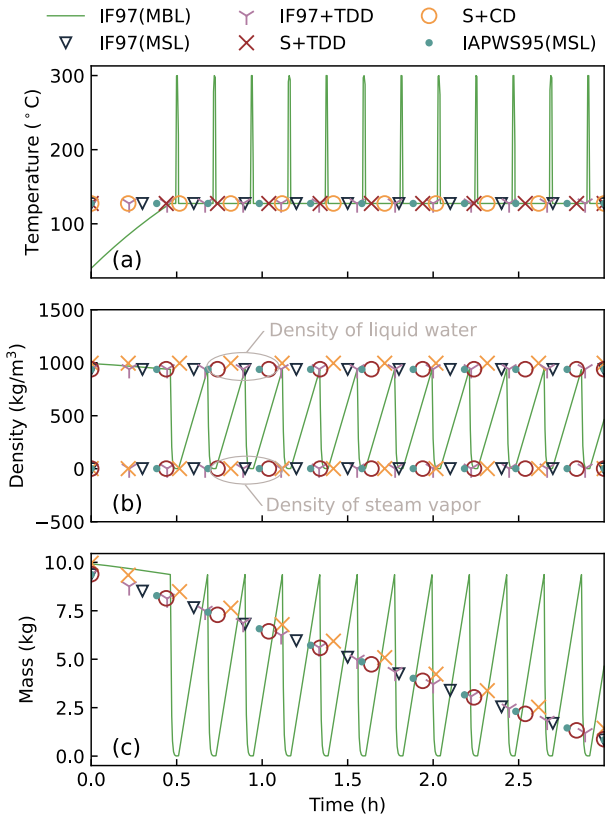

Figure 11: Evolution of (a) fluid temperature and (b) fluid density, including both the liquid and vapor components, and (c) fluid mass in the control volume through the boiling process.

of its design temperature range, causing higher than normal errors to be introduced. However, with that said the S+CW case did produce less than 1% errors in terms of CVRMSE for most property evaluations. The largest errors were introduced in the S+CW case for ρ_1 and m, with CVRMSE values of 5.9% and 7.6% respectively, while CVRMSE for IF97+TDD and S+TDD were less than 0.4% for all property evaluations. However, because boiling a volume of water completely is not a typical normal-operation scenario for DH applications, all of the split-medium models can be deemed acceptable.

4.2.2. Computing Speed

Table 7 presents the computing speed results for the control volume component evaluations. The computing speed for the IF97(MBL) case was significantly slower than all other cases, indicative of the chattering problem. Across the remaining five cases, the IAPWS95(MSL) case had the slowest computing time. Relative to IAPWS95(MSL), time savings of 18%, 25%, 37%, and 35% were achieved for the IF97(MSL), IF97+TDD, S+TDD, and S+CD cases, respectively. These trends are consistent with expectations, as computing times generally reduced as additional simplifications to the medium model implementations were made.

While the overall computing times for this small simulation case are notably small, the structure of the differential algebraic system of equations indicates the likelihood of computing speed differences for larger thermo-fluid system models. Except for IF97(MBL), the other five cases contain six continuous time state variables; however, the nonlinear systems of equations varies among these five cases. The IAPWS95(MSL) and IF97(MSL) cases each contain a nonlinear system with one iteration variable: dV_1/dt. Conversely, the new split-medium implementations (IF97+TDD, S+TDD, and S+CD) contain no nonlinear systems. While the nonlinear systems are small for this component-scale evaluation, their sizes and quantities will grow as DH system models increase in the number of buildings. From experiences, the time required to iteratively solve the nonlinear systems largely contribute to the total computing time. Thus, this likely will have an impact on computing time for DH applications, which will be quantitatively tested in the next section.

4.3. District Scale

Following the methodology prescribed in subsection 3.3, the results for model accuracy and numerical performance at the district scale evaluation are as follows. To evaluate impacts with respect to the number of buildings N, simulations are repeated with 1 to 10 buildings.

4.3.1. Accuracy

Figure 12 depicts the high accuracy achieved between the four cases for heat flow rate at each building, the fuel consumption rate at the boiler, and electric power at the feedwater pump. In Figure 12(a), the measured heat flow rate at the building for each of the four cases followed the input data file with minimal deviation (RMSE of 4 W and CVRMSE of 0.03% for all cases with respect to the input data). Given that the input to the building model was the data table and the condensate return pumps controlled the mass flow rate ideally, this was expected. In Figure 12(b) and (c), there are slight deviations in the boiler's fuel consumption rate and pump power across the four cases. For the boiler's fuel consumption rate, the IF97+TDD and S+TDD cases both produced RMSE of 5.3 kW (CVRMSE of 2.6%) compared to IF97(MSL), while the S+CD case produced RMSE of 7.1 kW (CVRMSE of 3.5%) compared to IF97(MSL). For feedwater pumping power, the S+CD case also produced slightly higher errors than the other two cases with CVRMSE of 4.2%, compared to 1.5% for IF97+TDD and S+TDD. These differences were primarily caused by deviations in the density at the pump inlet port ρ_1, which impacts pumping power as presented in section 2.3.1. For the feedwater pump inlet, the density RMSE and CVRMSE for IF97+TDD, S+TDD, and S+CD were 0.52 kg/m^3 (0.1%), 0.52 kg/m^3 (0.1%), and 37 kg/m^3 (4%), respectively. Over the two-day simulation period, the total boiler fuel consumption was within 1% error of the IF97(MSL) for all three split-medium cases. For the feedwater pump energy consumption, the IF97+TDD and S+TDD cases were within 0.3% of IF97(MSL), while the S+CD case produced 4% error.

As seen in Table 8 and Table 9, the accuracy of thermodynamic property evaluations at building 1 had insignificant differences across all cases. Here, the building 1 results are used as

Table 6: RMSE and CVRMSE of control volume evaluations relative to the IAPWS95(MSL) case.

Property	*RMSE*					*CVRMSE (%)*			
	S+CD	*S+TDD*	*IF97+TDD*	*IF97(MSL)*	*Units*	*S+CD*	*S+TDD*	*IF97+TDD*	*IF97(MSL)*
ρ_1	58.6	1.9	1.9	<0.001	kg/cm^3	5.9	0.2	0.2	<0.001
ρ_2	<0.001	<0.001	<0.001	<0.001	kg/cm^3	<0.001	<0.001	<0.001	<0.001
h	1.5	1.5	1.5	0.005	kJ/kg	0.06	0.06	0.06	<0.001
u	2.4	2.3	2.3	0.002	kJ/kg	0.4	0.4	0.4	<0.001
s	0.005	0.005	0.004	<0.001	kJ/kg-K	0.07	0.07	0.05	<0.001
T	<0.001	<0.001	<0.001	<0.001	K	<0.001	<0.001	<0.001	<0.001
m	0.6	0.02	0.02	<0.001	kg	7.6	0.3	0.3	<0.001

Table 7: Computing times for the boiler component evaluation with time savings relative to IAPWS95(MSL). Results are averages over 10 simulation runs.

Case	*Computing Time (s)*	*Time Savings (%)*
IAPWS95(MSL)	0.020	–
IF97(MSL)	0.016	18
IF97(MBL)	14.3	None
IF97+TDD	0.015	25
S+TDD	0.012	37
S+CD	0.013	35

Table 8: RMSE of building 1 thermodynamic properties from DH evaluations relative to IF97(MSL). Subscript 1 is for the inlet and 2 is for the outlet.

Property	*S+CD*	*S+TDD*	*IF97+TDD*	*Units*
T_1	0.007	0.007	0.001	K
p_1	7.49	8.58	5.79	Pa
h_1	1.74	1.74	0.001	kJ/kg
s_1	0.007	0.007	0.0	kJ/kg-K
T_2	0.017	0.017	0.017	K
p_2	7.49	8.58	5.79	Pa
h_2	2.79	2.79	2.79	kJ/kg
s_2	0.007	0.007	0.007	kJ/kg-K

proxies for all simulation cases, since the accuracy did not significantly change building to building, with respect to N, and at different points throughout the system. Subscripts 1 and 2 refer to the inlet and outlet ports of the building model, where the inlet state is steam vapor and the outlet state is liquid water condensate. As expected, the errors generally increased inversely to the steam/water model complexity. In this experiment, the IF97+TDD case produced the lowest errors compared to the IF97(MSL) case, followed by the S+TDD case. While the S+CD case produced some of the higher errors, all errors were within acceptable ranges. For example, the CVRMSE values are within 1% for all property evaluations. With the split-medium approaches, these DH simulations were able to produce acceptable accuracy for all thermodynamic property states.

Table 9: CVRMSE (%) of building 1 thermodynamic properties from DH evaluations relative to IF97(MSL). Subscript 1 is for the inlet and 2 is for the outlet.

Property	*S+CD*	*S+TDD*	*IF97+TDD*
T_1	0.002	0.002	0.0
p_1	0.002	0.003	0.002
h_1	0.064	0.064	0.0
s_1	0.11	0.11	0.0
T_2	0.004	0.004	0.004
p_2	0.002	0.003	0.002
h_2	0.50	0.50	0.50
s_2	0.40	0.40	0.40

4.3.2. Computing Speed

Table 10 presents the structure of the translated model for each of the four cases. The number of continuous time states did not vary across the four cases. However importantly, the split-medium approaches reduced the size of linear and nonlinear systems present in the district models. For the IF97(MSL) case, both the number of linear systems and the dimension of the largest nonlinear system increase with the N. Conversely, the linear and nonlinear systems do not change with respect to N for the three split-medium cases. Because solving nonlinear systems of equations are computationally expensive, these results are highly advantageous for simulations of large DH systems, especially when considering computing time requirements for industry applications.

The scaling results in Figure 13 clearly depict the computing speed benefits of the three split-medium approaches compared to the standard IF97(MSL) case. For large N, the computing time is expected to scale as $t_{cpu} = k\,N^p$, where k is some constant and p is the order of the scaling. On a log-log plot, this curve becomes $\log(t_{cpu}) = \log(k) + p \log N$. Making a data fit for $N \geq 100$, which is where we see the expected linear behavior reproduced in the data, we obtain for IF97(MSL) $p = 3.3$ (i.e., cubic scaling), while for IF97+TDD, S+TDD, and S+CD, p is 2.1, 2.3, and 2.1, respectively (i.e., quadratic scaling). Thus, the main computational advantages were not from the superheated steam simplifications (S), but from the numerically-efficient liquid water models (TDD or CD) with the split-medium approaches. This results was achieved by decoupling the mass and energy balances through the split-

Table 10: Translation results with respect to the number of buildings N in the DH system model. Results given are after Dymola's built-in model manipulation.

N	*Continuous*	*Linear Systems*				*Nonlinear Systems*			
	Time States	*IF97(MSL)*	*IF97+TDD*	*S+TDD*	*S+CD*	*IF97(MSL)*	*IF97+TDD*	*S+TDD*	*S+CD*
10	71	$\{2,2,...,2_{(11)}\}$	{2}	{2}	{2}	{11,4}	{3}	{3}	{1}
20	131	$\{2,2,...,2_{(21)}\}$	{2}	{2}	{2}	{21,4}	{3}	{3}	{1}
30	191	$\{2,2,...,2_{(31)}\}$	{2}	{2}	{2}	{31,4}	{3}	{3}	{1}
⋮	⋮	⋮	⋮	⋮	⋮	⋮	⋮	⋮	⋮
n	$6n + 11$	$\{2,2,...,2_{(n+1)}\}$	{2}	{2}	{2}	$\{n + 1,4\}$	{3}	{3}	{1}

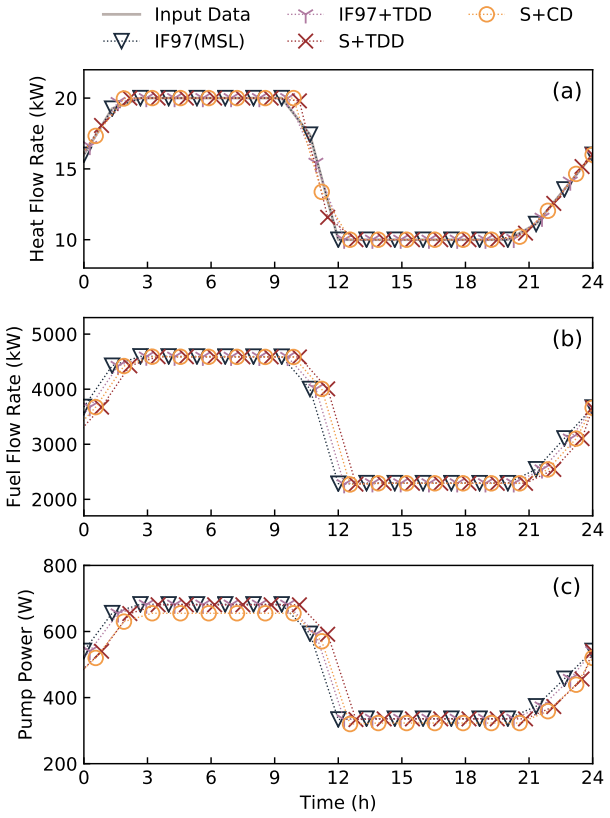

Figure 12: Accuracy evaluation for district scale results including (a) heat flow rate at each building compared to the input data file, (b) boiler fuel consumption rate, and (c) feedwater pump power. Input data refers to the prescribed heat flow rate at each building and thus only appears in (a).

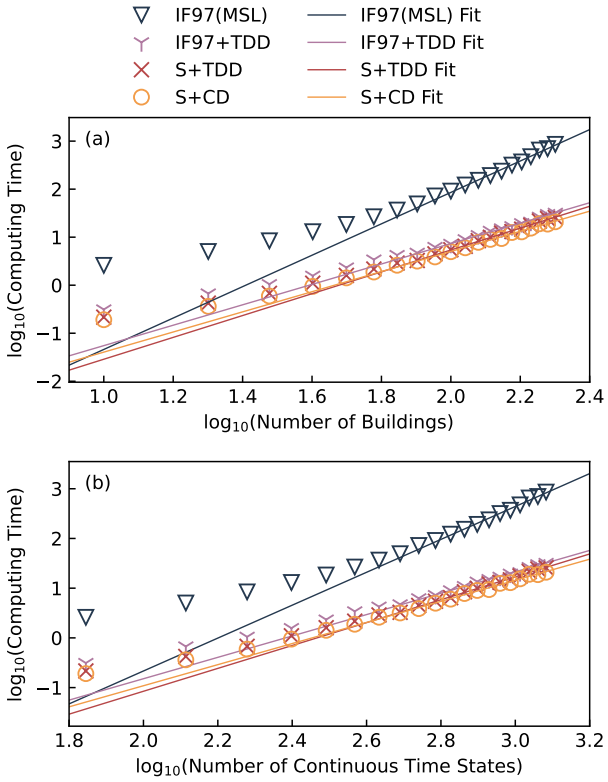

Figure 13: Computing time in seconds, presented on a log-log scale (base 10), with respect to (a) the total number of interconnected buildings N and (b) the number of continuous time states. Linear fits indicating scaling rates are shown for $N \in [100, 200]$.

medium approach, which eliminated costly nonlinear systems of equations. As an example, the computing time for an annual simulation with 180 buildings will improve from 33 hours with IF97(MSL) to 1-1.5 hours with the split-medium implementations. These results are critically important to enable industry to simulate complete steam DH systems at large scales.

5. Discussion

To our knowledge, this is the first modeling and simulation setup for complete steam DH systems featuring a plant, a distribution network, interconnected buildings with closed fluid loops and feedback control, which can also be coupled to building models of various levels of detail or to electrical system models which are part of the MBL [7, 55, 56]. As complete steam DH systems present new computational challenges, particularly at large scale, we focus on the modeling of water/steam thermodynamics, which affects both accuracy and computing speed across scales. We propose a novel split-medium approach that couples numerically efficient liquid water models with various water/steam models and evaluate performance across thermodynamic property, component, and district scales. As a first of its kind for steam DH systems, there are several important limitations to consider and opportunities for improvement.

First, at the thermodynamic property scale, the accuracy of

the TDD and CD liquid water models from the MBL were evaluated with respect to IF97 and IAPWS-95. This study extended these models beyond their original design intention, thus revealing that they are most suitable for pressures less than 4 MPa. This upper pressure limit was most restricted by the constant c_p assumption, which produced errors as high as 11.8% under high temperature and pressure conditions. If the TDD model were to be improved in the future, changing the c_p function from constant to a temperature-dependent polynomial function likely can increase the upper pressure limit with minimal impacts to numerical performance. This hypothesis can be evaluated in the future. Further, this study focused on analytical models for thermodynamic properties rather than table-based methods. It is possible that the table-based methods can outperform analytical models for steam DH systems. This has yet to be studied and can be evaluated in the future.

Second, the component scale evaluation revealed that errors in internal energy and mass calculations increase as mass goes to zero. This is an atypical scenario in normal operation, because boilers are controlled to maintain a water level setpoint. However, it is important to recognize modeling sensitivity at low mass quantities and mass flow rates, particularly with large, complex, DH system models where problems can be difficult to diagnose. One solution to this problem can be to include smoothing functions that account for regularization at low mass conditions to avoid diverging extensive property evaluations.

Third, the district scale evaluation importantly revealed how the split-medium approaches can reduce the computing time from cubic to quadratic with negligible compromise to accuracy. While additional time savings with the simplified steam vapor model (S) and liquid water model (CD) are possible, the most significant benefits can be achieved with the IF97+TDD case. This finding is critical for practical applications of steam DH simulations in industry, particularly since the IF97+TDD case had the largest *p-T* applicable range of all split-medium approaches.

However, as a first of its kind demonstration, simplifying assumptions were made in the complete steam DH model that present opportunities for improvement in the future. Most notably, only the pressure drop in the condensate return pipes of the distribution network were included, while the steam supply pipes were lossless. To our knowledge, a model for a saturated steam pipe with a drip-leg that can accommodate both pressure and heat losses is not available. Indeed, the Termis software [39] cannot model saturated steam pipes nor condensation in the distribution network. Although this lossless assumption was appropriate based on this study's objectives, it is unrealistic for real-world case studies, since heat and pressure losses are not negligible in both the steam supply and condensate return pipes, and mass losses are not negligible in steam pipes. With that said, we are currently developing a model for a steam supply pipe (saturated or superheated) with a drip-leg for condensate return, which will be made publicly available in the future. For saturated or superheated steam pipes with condensation, the steam supply with drip-leg model instantiates the saturated control volume (section 2.3.3) developed herein. Meanwhile, for superheated steam supply pipes without condensation, several pipe models are readily available (e.g., the MBL plug flow pipe).

In addition, the studied system at district scale included steam traps that vent to atmospheric pressure, which decreased the pressures of subcooled liquid water. While this is a common system design, some systems implement high pressure steam traps or have flash tanks that can increase the back pressure downstream of the steam trap; based on the thermodynamic scale results herein, these higher pressure states for liquid condensate have lower accuracy with the TDD and CD models. This can correspond to lower accuracy in pumping power and boiler fuel consumption rate. With the IF97+TDD case as currently designed, the split-medium approach is currently limited to 0-4 MPa for subcooled liquid condensate, while the full 0-100 MPa are retained for all other water/steam phases. Lastly, a single plant configuration was included in this study, representing one of the more simple designs. Future work will include more advanced plant configurations and controls.

6. Conclusion

With district-scale simulations growing in importance as societies strive to meet energy and climate targets, this work enables the modeling and simulation of complete steam-based DH systems that, for all intents and purposes, was not previously possible for industry applications. Based on the medium models considered, the IF97+TDD performed the best in terms of both accuracy and computing speed for complete steam DH simulations at large scales, reducing the computing time scaling rate from cubic to quadratic while maintaining accuracies within 3.5% CVRMSE across energy, power, and fuel consumption rate calculations. The significant computing time savings were achieved by replacing the subcooled liquid water region of the IF97 model with a numerically efficient model from the MBL, as the medium model in the MBL allows Modelica translators to formulate a differential equation for the system model in which mass and energy balance are decoupled. This avoids costly nonlinear systems of equations. These results are critically important to enable industry practitioners to simulate complete steam DH systems at large scales. While there is room for improvement in the models from thermodynamic properties through complete systems, the split-medium approach can help aid the transition of legacy DH systems to newer sustainable designs, while providing a pathway for practical district-scale analysis and optimization in the many steam heating applications that are likely to remain.

7. Acknowledgements

This research was supported in part by an appointment with IBUILD Graduate Student Research Program sponsored by the U.S. Department of Energy (DOE), Office of Energy Efficiency and Renewable Energy, and Building Technologies Office. This program is managed by Oak Ridge National Laboratory (ORNL). This program is administered by the Oak Ridge Institute for Science and Education (ORISE) for the DOE.

ORISE is managed by ORAU under DOE contract number DESC0014664. All opinions expressed in this paper are the author's and do not necessarily reflect the policies and views of DOE, ORNL, ORAU, or ORISE. In addition, this material is based upon work supported by the DOE's Office of Energy Efficiency and Renewable Energy under the Advanced Manufacturing Office, award number DE-EE0009139, and the Building Technologies Office, contract number DE-AC02-05CH11231. Further, this work emerged from the IBPSA Project 1, an international project conducted under the umbrella of the International Building Performance Simulation Association (IBPSA). Project 1 will develop and demonstrate a BIM/GIS and Modelica Framework for building and community energy system design and operation.

8. Disclaimer

Appendix A. IAPWS-95

The primary innovations of this work include the split-medium approach and numerically efficient component models. We then simulated complete steam DH systems at large scales, which to our knowledge, is novel among existing literature. Consistent with [8, 57], we provide additional details regarding the mathematical formulations of water/steam used in this work in appendices. In this work, we implement the IAPWS-95 formulation [8] in Modelica for comparative evaluation. This formulation includes a single-set of equations explicit in the Helmholtz free energy f with density ρ and temperature T as independent variables. The fundamental equation expresses the dimensionless form of the Helmholtz free energy ϕ in terms of the ideal-gas part ϕ° and residual part ϕ^r as

$$\phi(\delta,\tau) = \frac{f(\rho,T)}{RT} = \phi^\circ(\delta,\tau) + \phi^r(\delta,\tau), \tag{A.1}$$

where the reduced density $\delta = \rho/\rho_c$ and the reduced temperature $\tau = T_c/T$, with subscript c indicating critical points. For reference, the critical density and temperature for water are 322 kg/m^3 and 647.096 K, respectively.

The form of the ideal-gas part ϕ° is

$$\phi^\circ = \ln\delta + n_1^\circ + n_2^\circ\tau + n_3^\circ \ln\tau + \sum_{i=4}^{8} n_i^\circ \ln\left[1-\exp\left(-\gamma_i^\circ\tau\right)\right], \tag{A.2}$$

where each of the 8 coefficients for n_i° and exponents γ_i° are tabulated in Table 1 of [8]. Similarly, the form of the residual part ϕ^r is

$$\begin{aligned}
\phi^r \quad &= \quad \sum_{i=1}^{7} n_i\delta^{d_i}\tau^{t_i} + \sum_{i=8}^{51} n_i\delta^{d_i}\tau^{t_i}\exp\left(-\delta^{c_i}\right) && \text{(A.3)}\\
&+ \quad \sum_{i=52}^{54} n_i\delta^{d_i}\tau^{t_i}\exp\left(-\alpha_i(\delta-\varepsilon_i)^2 - \beta_i(\tau-\gamma_i)^2\right)\\
&+ \quad \sum_{i=55}^{56} n_i\Delta^{b_i}\delta\psi,\\
\text{with} \quad \Delta \quad &= \quad \theta^2 + B\left[(\delta-1)^2\right]^{a_i}, && \text{(A.4)}\\
\theta \quad &= \quad (1-\tau) + A_i\left[(\delta-1)^2\right]^{\frac{1}{2\beta_i}}, \quad \text{and} && \text{(A.5)}\\
\psi \quad &= \quad \exp\left(-C_i(\delta-1)^2 - D_i(\tau-1)^2\right), && \text{(A.6)}
\end{aligned}$$

where each of the coefficients and parameters for c_i, d_i, t_i, α_i, β_i, γ_i, ε_i, A_i, C_i, and D_i are tabulated in Table 2 of [8].

Based on the ideal-gas and residual parts of the dimensionless Helmholtz free energy and their derivatives, thermodynamic properties are calculated. Each of the following derivatives are tabulated in Table 4 (ideal-gas part) and Table 5 (residual part) of [8]. By definition, pressure $p = \rho^2(\partial f/\partial\rho)_T$, and the IAPWS-95 relation is

$$\frac{p(\delta,\tau)}{\rho RT} = 1 + \delta\left[\frac{\partial\phi^r}{\partial\delta}\right]_\tau. \tag{A.7}$$

Internal energy is defined in terms of the Helmholtz free energy as $u = f - T(\partial f/\partial T)_\rho$, and the relation to the dimensionless form is

$$\frac{u(\delta,\tau)}{RT} = \tau\left(\left[\frac{\partial\phi^\circ}{\partial\tau}\right]_\delta + \left[\frac{\partial\phi^\circ}{\partial\tau}\right]_\delta\right). \tag{A.8}$$

Similarly, specific enthalpy, $h = f - T(\partial f/\partial T)_\rho + \rho(\partial f/\partial\rho)_T$, and specific entropy, $s = -(\partial f/\partial T)_\rho$, are calculated in IAPWS-95 with

$$\frac{h(\delta,\tau)}{RT} = 1 + \tau\left(\left[\frac{\partial\phi^\circ}{\partial\tau}\right]_\delta + \left[\frac{\partial\phi^\circ}{\partial\tau}\right]_\delta\right) + \delta\left[\frac{\partial\phi^r}{\partial\delta}\right]_\tau, \tag{A.9}$$

and

$$\frac{s(\delta,\tau)}{R} = \tau\left(\left[\frac{\partial\phi^\circ}{\partial\tau}\right]_\delta + \left[\frac{\partial\phi^\circ}{\partial\tau}\right]_\delta\right) - \phi^\circ - \phi^r. \tag{A.10}$$

Formulations for other thermodynamic properties in terms of the dimensionless Helmholtz free energy are in Table 3 of [8]. These include the isochoric heat capacity c_v, isobaric heat capacity c_p, and the Maxwell criterion for the phase-equilibrium conditions, among others.

Appendix B. IF97 Region 2 Equations

Complete details for the IF97 formulation of water and steam are available in [9, 57]. However, to provide a reference point for the functions we replaced with the superheated steam approximations (Appendix C), relevant formulations for specific enthalpy and entropy are reproduced here. In the IF97 formulation for Region 2 (superheated vapor, referred as region 5 in this work), basic equations for Gibbs free energy g are expressed in a dimensionless form

$$\gamma(\pi,\tau) = \frac{g(p,T)}{RT} = \gamma^{\circ}(\pi,\tau) + \gamma^{r}(\pi,\tau), \tag{B.1}$$

where γ° represents the ideal-gas part and γ^{r} represents the residual part. This equation is formulated in terms of the specific gas constant of ordinary water $R = 0.461526\,\mathrm{kJ/(kg\cdot K)}$, the reduced pressure $\pi = p/p^{*}$, and the inverse reduced temperature $\tau = T^{*}/T$, where superscript * indicates the reducing quantity. For these equations, $p^{*} = 1$ MPa and $T^{*} = 540$ K.

The form of the ideal-gas part γ° is

$$\gamma^{\circ}(\pi,\tau) = \ln\pi + \sum_{i=1}^{9} n_i^{\circ}\tau^{J_i^{\circ}}, \tag{B.2}$$

where each of the 9 coefficients for n_i° and J_i° are tabulated in Table 10 of [57]. Similarly, the form of the residual part γ^{r} is given as

$$\gamma^{r}(\pi,\tau) = \sum_{i=1}^{43} n_i\pi^{I_i}(\tau-0.5)^{J_i}, \tag{B.3}$$

where each of the 43 coefficients for n_i and exponents I_i and J_i are tabulated in Table 11 of [57].

In terms of Gibbs free energy, specific enthalpy $h = g - T(\partial g/\partial T)_p$. Thus, the dimensionless relation in terms of the ideal-gas and residual parts can be expressed as

$$\frac{h(\pi,\tau)}{RT} = \tau\left(\left[\frac{\partial\gamma^{\circ}}{\partial\tau}\right]_{\pi} + \left[\frac{\partial\gamma^{r}}{\partial\tau}\right]_{\pi}\right), \tag{B.4}$$

where the partial derivatives of γ° and γ^{r} with respect to τ at constant π are

$$\left[\frac{\partial\gamma^{\circ}}{\partial\tau}\right]_{\pi} = \sum_{i=1}^{9} n_i^{\circ}J_i^{\circ}\tau^{J_i^{\circ}-1} \quad \text{and} \tag{B.5}$$

$$\left[\frac{\partial\gamma^{r}}{\partial\tau}\right]_{\pi} = \sum_{i=1}^{43} n_i\pi^{I_i}J_i(\tau-0.5)^{J_i-1}. \tag{B.6}$$

In terms of Gibbs free energy, specific entropy $s = -(\partial g/\partial T)_p$, and the IF97 relation is

$$\frac{s(\pi,\tau)}{R} = \tau\left(\left[\frac{\partial\gamma^{\circ}}{\partial\tau}\right]_{\pi} + \left[\frac{\partial\gamma^{r}}{\partial\tau}\right]_{\pi}\right) - (\gamma^{\circ}+\gamma^{r}). \tag{B.7}$$

This completes the forward equations for $h(p,T)$ and $s(p,T)$ in the IF97 formulation, Region 2. In total, $h(p,T)$ includes 5 equations, 52 coefficients, and 95 exponents, while $s(p,T)$ includes 7 equations, 104 coefficients, and 190 exponents. In addition to the forward equations, separate backward equations are similarly implemented. However, Region 2 is further divided into three subregions 2a, 2b, and 2c (see [57] for subregion divisions). Thus, three $T(p,h)$ and three $T(p,s)$ cover Region 2, but only subregion 2a is applicable for the reduced p-T range specified for DH applications in Table 1. The dimensionless backward equation $T(p,h)$ for subregion 2a is

$$\frac{T(p,h)}{T^{*}} = \sum_{i=1}^{34} n_i\pi^{I_i}(\eta-2.1)^{J_i}, \tag{B.8}$$

where $\eta = h/h^{*}$, $h^{*} = 2000$ kJ/kg, and each of the 34 coefficients for n_i and exponents I_i and J_i are tabulated in Table 20 of [57].

Lastly, the backward function $T(p,s)$ for subregion 2a is

$$\frac{T(p,s)}{T^{*}} = \sum_{i=1}^{46} n_i\pi^{I_i}(\sigma-2)^{J_i}, \tag{B.9}$$

where $\sigma = s/s^{*}$, $s^{*} = 2\,\mathrm{kJ/(kg\cdot k)}$, and each of the 46 coefficients for n_i and exponents I_i and J_i are tabulated in Table 25 of [57]. In total, $T(p,h)$ includes 34 coefficients and 68 exponents, while $T(p,s)$ includes 46 coefficients and 92 exponents. Modelica implementations of the above forward and backward equations for specific enthalpy and entropy along with the other thermodynamic properties are used for comparative evaluation in this study.

Appendix C. Superheated Steam Approximations

To evaluate the potential numerical benefits of reduced-order polynomial approximations for superheated steam thermodynamics, we replaced commonly called thermodynamic functions in the formulation of medium model S. Because this endeavor was a secondary evaluation beyond the split-medium approach, we include the mathematical details for these approximations in the appendix. In energy and exergy analysis of steam DH systems, specific enthalpy h and specific entropy s are frequently called. Thus, we replace these two functions with invertible polynomial approximations such that $h(p,T(p,h^{*})) = h^{*}$ for any $p,h^{*} \in \mathfrak{R}$. Polynomial coefficients are determined via a linear least squares method for two-dimensional polynomial surface fits. The goal of this is not only to reduce the computational load through lower-order functions, but also to avoid numerical challenges due to inconsistent forward and backward equations in the IF97 formulation. First, to minimize the sensitivity to round off errors and alleviate numerical problems, we improve the conditioning of input variables pressure and temperature by centering and scaling the inputs to standard-normal distributions using

$$\overline{p} = \frac{p - p_{mean}}{p_{sd}} \quad \text{and} \tag{C.1}$$

$$\overline{T} = \frac{T - T_{mean}}{T_{sd}}, \tag{C.2}$$

where $\overline{p}$ and $\overline{T}$ are the normalized pressure and temperature, respectively; and subscripts *mean* and *sd* signify the mean and standard deviation, respectively, of the selected input data set. A dense input grid was developed at standard increments of 0.1 K and 1 kPa from the IF97 formulation. Several invertible polynomials were evaluated before selecting (1) the lowest order fits and (2) an acceptable reduced p-T range with acceptable accuracy and suitability for industrial applications. Based on this process, the following pressure and temperature ranges were selected for this reduced range implementation

$$0.1 \leq p \leq 0.55\,\text{MPa} \quad \text{and} \tag{C.3}$$

$$100 \leq T \leq 160\,^{\circ}\text{C}. \tag{C.4}$$

Table C.11 presents the normalization parameters used that pertain to the selected p-T input grid for the polynomial approximations.

Table C.11: Normalization parameters for polynomial approximations.

Parameter	*Value*	*Units*
p_{mean}	1.235e+06	Pa
p_{sd}	8.326e+05	Pa
T_{mean}	6.776e+02	K
T_{sd}	1.611e+02	K

For specific enthalpy, we selected a linear approximation $\hat{h}(p,T) \approx h(p,T)$, with $h(p,T)$ given in Equation B.4, as

$$\hat{h}(p,T) = a_1 + a_2\overline{p} + a_3\overline{T}, \tag{C.5}$$

where h is specific enthalpy and a_i are regression coefficients. The corresponding backward equation is formulated directly from Equation C.5 by solving for T as

$$T(p,h) = c_1 + c_2\overline{p} + c_3 h, \tag{C.6}$$

where

$$\boldsymbol{c} = [c_1, c_2, c_3] = \left[\frac{-a_1 T_{sd}}{a_3 T_{mean}}, \frac{-a_2 T_{sd}}{a_3}, \frac{T_{sd}}{a_3}\right]. \tag{C.7}$$

Table C.12 lists the regression coefficients for Equation C.5 found using this least squares approach.

Table C.12: Regression coefficients for specific enthalpy $h(p,T)$ and $T(p,h)$.

Parameter	*Value*	*Units*
a_1	3.272e+06	kJ/kg
a_2	-1.838e+04	kJ/kg-Pa
a_3	3.504e+05	kJ/kg-K

Similar to specific enthalpy, we selected an invertible polynomial approximation for specific entropy $\hat{s}(p,T) \approx s(p,T)$, with $s(p,T)$ given in Equation B.7. Using a function that is quadratic in pressure and linear in temperature, specific entropy can be approximated as

$$\hat{s}(p,T) = d_1 + d_2\overline{p} + d_3\overline{T} + \overline{p}(d_4\overline{p} + d_5\overline{T}), \tag{C.8}$$

where s is specific entropy and d_i are regression coefficients. While higher order models could produce better fits, Equation C.8 was selected because its accuracy was sufficient while still meeting our goal of having invertible functions. Solving for T directly from Equation C.8, we write the backward function as

$$T(p,s) = \frac{(s - d_1 - \overline{p}(d_2 + d_4\overline{p}))T_{sd}}{d_3 + d_5\overline{p}} + T_{mean}. \tag{C.9}$$

Regression coefficients for Equation C.8 are listed in Table C.13.

Table C.13: Regression coefficients for specific entropy $s(p,T)$ and $T(p,s)$.

Parameter	*Value*	*Units*
d_1	7530	kJ/kg-K
d_2	-636.9	kJ/kg-K-Pa
d_3	532.8	kJ/kg-K^2
d_4	159.8	kJ/kg-K-Pa^2
d_5	4.130	kJ/kg-K^2-Pa

References

[1] D. Connolly, H. Lund, B. V. Mathiesen, S. Werner, B. Möller, U. Persson, T. Boermans, D. Trier, P. A. Østergaard, S. Nielsen, Heat roadmap Europe: Combining district heating with heat savings to decarbonise the EU energy system, Energy Policy 65 (2014) 475–489. doi:10.1016/j.enpol.2013.10.035.

[2] S. Frederiksen, S. Werner, District Heating and Cooling, 1st Edition, Studentlitteratur AB, Lund, Sweden, 2013.

[3] ICF LLC, International District Energy Association, U.S. District Energy Services Market Characterization, Tech. rep., U.S. Energy Information Administration, Washington DC (2018).
URL https://www.eia.gov/analysis/studies/buildings/districtservices/pdf/districtservices.pdf

[4] I. BCS, Waste Heat Recovery: Technology Opportunities in the US Industry, Tech. rep. (2008).
URL http://www1.eere.energy.gov/manufacturing/intensiveprocesses/pdfs/waste_heat_recovery.pdf

[5] N. Long, A. Gautier, H. Elarga, A. Allen, T. Summer, L. Klun, N. Moore, M. Wetter, Modeling district heating and cooling systems with URBANopt , GeoJSON to Modelica Translator , and the Modelica Buildings Library, in: Building Simulation Conference, Bruges, Belgium, 2021.

[6] R. E. Kontar, B. Polly, T. Charan, K. Fleming, N. Moore, N. Long, D. Goldwasser, URBANopt: An Open-source Software Development Kit for Community and Urban District Energy Modeling, in: Building Performance Analysis Conference and SimBuild, 2020.

[7] M. Wetter, W. Zuo, T. S. Nouidui, X. Pang, Modelica Buildings library, Journal of Building Performance Simulation 7 (4) (2014) 253–270. doi:10.1080/19401493.2013.765506.

[8] International Association for the Properties of Water and Steam, Revised Release on the IAPWS Formulation 1995 for the Thermodynamic Properties of Ordinary Water Substance for General and Scientific Use, Tech. rep., International Association for the Properties of Water and Steam, Prague, Czech Republic (2018). doi:10.1063/1.1461829.

[9] W. Wagner, J. R. Cooper, A. Dittmann, J. Kijima, H. J. Kretzschmar, A. Kruse, R. Mareš, K. Oguchi, H. Sato, I. Stöcker, O. Šifner, Y. Takaishi, I. Tanishita, J. Trübenbach, T. Willkommen, The IAPWS industrial formulation 1997 for the thermodynamic properties of water and steam,

Journal of Engineering for Gas Turbines and Power 122 (1) (2000) 150–180. doi:10.1115/1.483186.

[10] M. Åberg, Optimisation-friendly modelling of thermodynamic properties of media, Msc thesis, Lund University (2016).

[11] R. Hofmann, P. Linzner, H. Walter, T. Will, New approximation algorithms for the state functions of water and steam for the application of transient processes and fast on-line applications, Energy 164 (2018) 1079–1096. doi:10.1016/j.energy.2018.09.039.

[12] M. Affandi, N. Mamat, S. N. A. M. Kanafiah, N. S. Khalid, Simplified equations for saturated steam properties for simulation purpose, Procedia Engineering 53 (Malaysian Technical Universities Conference on Engineering & Technology 2012) (2013) 722–726. doi:10.1016/j.proeng.2013.02.095.

[13] J. G. Fonseca, P. S. Schneider, Simulation of a thermal power plant with district heating: Comparative results of 5 different codes, Energy 31 (12) (2006) 1955–1968. doi:10.1016/j.energy.2005.08.011.

[14] J. Bonilla, L. J. Yebra, S. Dormido, A heuristic method to minimise the chattering problem in dynamic mathematical two-phase flow models, Mathematical and Computer Modelling 54 (5-6) (2011) 1549–1560. doi:10.1016/j.mcm.2011.04.026.

[15] R. Sangi, P. Jahangiri, A. Thamm, D. Müller, Dynamic exergy analysis – Modelica®-based tool development: A case study of CHP district heating in Bottrop, Germany, Thermal Science and Engineering Progress 4 (July) (2017) 231–240. doi:10.1016/j.tsep.2017.10.008.

[16] International Association for the Properties of Water and Steam, Guideline on the Fast Calculation of Steam and Water with the Spline-Based Table Look-up Method (SBTL), Tech. Rep. IAPWS G13-15, The International Association for the Properties of Water and Steam, Stockholm, Sweden (2015).

[17] M. De Lorenzo, P. Lafon, M. Di Matteo, M. Pelanti, J. M. Seynhaeve, Y. Bartosiewicz, Homogeneous two-phase flow models and accurate steam-water table look-up method for fast transient simulations, International Journal of Multiphase Flow 95 (2017) 199–219. doi:10.1016/j.ijmultiphaseflow.2017.06.001.

[18] J. Bonilla, L. J. Yebra, E. Zarza, S. Dormido, Chattering in dynamic mathematical two-phase flow models, Applied Mathematical Modelling 36 (2012) 2067–2081. doi:10.1016/j.apm.2011.08.013.

[19] X. D. Wang, B. An, Y. Y. Duan, Z. X. Wang, D. J. Lee, Efficient and accurate computation scheme of p-T thermodynamic properties of water and steam, Journal of the Taiwan Institute of Chemical Engineers 43 (6) (2012) 845–851. doi:10.1016/j.jtice.2012.07.007.

[20] K. Miyagawa, P. G. Hill, A Tabular Taylor Series Expansion Method for Fast Calculation of Steam Properties, Journal of Engineering for Gas Turbines and Power 119 (April) (1997) 485–491.

[21] International Association for the Properties of Water and Steam, Guideline on the Tabular Taylor Series Expansion (TTSE) Method for Calculation of Thermodynamic Properties of Water and Steam, Tech. Rep. IAPWS G6-03, The International Association for the Properties of Water and Steam, Vejle, Denmark (2003).

[22] R. Berry, L. Zou, H. Zhao, H. Zhang, J. Peterson, R. Martineau, S. Kadioglu, D. Andrs, RELAP-7 Theory Manual (2016).

[23] United States Nuclear Regulatory Commission, TRACE V5. 0 Theory Manual: Field Equations, Solution Methods and Physical Models, Tech. rep., Washington, DC 20555-0001 (2012).

[24] CEA, EDF, FRAMATOME, CATHARE: Thermal-hydraulic simulation of multiphase flow dynamics (2022).
URL https://cathare.cea.fr/

[25] National Institute of Standards and Technology, REFPROPNIST Reference Fluid Thermodynamic and Transport Properties Database (REFPROP): Version 10 (2022).

[26] Gesellschaft für Anlagen- und Reaktorsicherheit, ATHELT 3.2: Program Overview (February) (2019).

[27] S. Tuuri, Apros Thermal: High fidelity dynamic simulation of thermal power plants, Tech. rep., Fortum, Finland (2019).

[28] X. Zhong, X. Zhang, M. Saeed, Z. Li, J. Yu, Comparative study on water thermodynamic property functions of TRACE code, Annals of Nuclear Energy 147 (2020) 107754. doi:10.1016/j.anucene.2020.107754.

[29] J. Beiron, R. M. Montañés, F. Normann, F. Johnsson, Dynamic modeling for assessment of steam cycle operation in waste-fired combined heat and power plants, Energy Conversion and Management 198 (August) (2019) 111926. doi:10.1016/j.enconman.2019.111926.

[30] Modelon, Thermal Power Library - Modelon (2019).
URL https://www.modelon.com/library/thermal-power-library/

[31] Z. Huang, C. Yang, H. Yang, X. Ma, Off-design heating/power flexibility for steam injected gas turbine based CCHP considering variable geometry operation, Energy 165 (2018) 1048–1060. doi:10.1016/j.energy.2018.09.126.

[32] Z. Zhang, L. Duan, Z. Wang, Y. Ren, General performance evaluation method of integrated solar combined cycle (ISCC) system, Energy 240 (2022) 122472. doi:10.1016/j.energy.2021.122472.

[33] K. Braimakis, D. Magiri-Skouloudi, D. Grimekis, S. Karellas, Energy-exergy analysis of ultra-supercritical biomass-fuelled steam power plants for industrial CHP, district heating and cooling, Renewable Energy 154 (2020) 252–269. doi:10.1016/j.renene.2020.02.091.

[34] F. Guo, X. Zhu, P. Li, X. Yang, Low-grade industrial waste heat utilization in urban district heating: Simulation-based performance assessment of a seasonal thermal energy storage system, Energy 239 (2022) 122345. doi:10.1016/j.energy.2021.122345.

[35] F. Sun, L. Fu, J. Sun, S. Zhang, A new waste heat district heating system with combined heat and power (CHP) based on ejector heat exchangers and absorption heat pumps, Energy 69 (2014) 516–524. doi:10.1016/j.energy.2014.03.044.

[36] M. Liu, M. Liu, Y. Wang, W. Chen, J. Yan, Thermodynamic optimization of coal-fired combined heat and power (CHP) systems integrated with steam ejectors to achieve heat–power decoupling, Energy 229 (2021) 120707. doi:10.1016/j.energy.2021.120707.

[37] L. Nielsen, ClaRa+ - System Simulation for new Energy Markets, Tech. rep., TLK-Thermo GmbH, Braunschweig, Germany (2021).
URL claralib.com/pdf/ClaRa_Flyer_Software.pdf

[38] B. El Hefni, D. Bouskela, Modeling and Simulation of Thermal Power Plants with ThermoSysPro: A Theoretical Introduction and a Practical Guide, Springer, Cham, Switzerland, 2019. doi:10.1007/978-3-030-05105-1_6.

[39] Schneider Electric, Termis District Energy Management: User Guide Version 5.0 (Q4) (2012).
URL https://download.schneider-electric.com/files?p_enDocType=User+guide&p_File_Name=Termis_5_0.pdf&p_Doc_Ref=Termis+Set+Up+Guide

[40] L. Wang, S. Yu, F. Kong, X. Sun, Y. Zhou, W. Zhong, X. Lin, A study on energy storage characteristics of industrial steam heating system based on dynamic modeling, Energy Reports 6 (2020) 190–198. doi:10.1016/j.egyr.2020.07.001.

[41] H. Wang, H. Wang, T. Zhu, W. Deng, A novel model for steam transportation considering drainage loss in pipeline networks, Applied Energy 188 (2017) 178–189. doi:10.1016/j.apenergy.2016.11.131.

[42] P. Jie, W. Zhao, F. Li, F. Wei, J. Li, Optimizing the pressure drop per unit length of district heating piping networks from an environmental perspective, Energy 202 (2020) 117681. doi:10.1016/j.energy.2020.117681.

[43] United States Department of Energy, Steam Systems and Component Models, in: EnergyPlus Version 8.9.0 Documentation: Engineering Reference, 2018, Ch. 9.10, pp. 482–497.

[44] J. Allegrini, K. Orehounig, G. Mavromatidis, F. Ruesch, V. Dorer, R. Evins, A review of modelling approaches and tools for the simulation of district-scale energy systems, Renewable and Sustainable Energy Reviews 52 (2015) 1391–1404. doi:10.1016/J.RSER.2015.07.123.

[45] G. Schweiger, R. Heimrath, B. Falay, K. O'Donovan, P. Nageler, R. Pertschy, G. Engel, W. Streicher, I. Leusbrock, District energy systems: Modelling paradigms and general-purpose tools, Energy 164 (2018) 1326–1340. doi:10.1016/J.ENERGY.2018.08.193.

[46] F. Bünning, M. Wetter, M. Fuchs, D. Müller, Bidirectional low temperature district energy systems with agent-based control: Performance comparison and operation optimization, Applied Energy 209 (2018) 502–515. doi:10.1016/j.apenergy.2017.10.072.

[47] J. Simonsson, K. T. Atta, G. Schweiger, W. Birk, Experiences from city-scale simulation of thermal grids, Resources 10 (2) (2021) 1–20. doi:10.3390/resources10020010.

[48] L. Li, J. Gohl, J. Batteh, C. Greiner, K. Wang, Fast Calculation of Refrigerant Properties in Vapor Compression Cycles Using Spline-Based Table Look-Up Method (SBTL), in: The American Modelica Conference, Cambridge, MA, USA, 2018, pp. 77–84. doi:10.3384/ecp1815477.

[49] Modelica Association, Modelica Standard Library - Version 3.2.3 (2019). URL https://doc.modelica.org/Modelica3.2.3/Resources/helpDymola/Modelica.html

[50] F. M. Marquez, P. J. Zufiria, L. J. Yebra, Port-Hamiltonian Modeling of Thermofluid Systems and Object-Oriented Implementation with Modelica I: Thermodynamic Part, IEEE Access 9 (2021) 131496–131519. doi:10.1109/ACCESS.2021.3115038.

[51] Modelica Association, Modelica Users Guide: Medium Definition (2020).
URL https://doc.modelica.org/Modelica4.0.0/Resources/helpWSM/Modelica/Modelica.Media.UsersGuide.MediumDefinition.html

[52] M. Wetter, Fan and Pump Model that has a Unique Solution for any Pressure Boundary Condition and Control Signal, in: The 13th Conference of International Building Performance Simulation Association, Chambéry, France, 2013, pp. 3505–3512.

[53] J. Astrom, K., D. Bell, R., Drum-boiler dynamics, Automatica 36 (2000) 363–378.

[54] X. Wu, J. Shen, Y. Li, K. Y. Lee, Steam power plant configuration, design, and control, WIREs: Energy and Environment 4 (6) (2015) 537–563. doi:10.1002/wene.161.

[55] M. Wetter, K. Benne, B. Ravache, Software Architecture and Implementation of Modelica Buildings Library Coupling for Spawn of EnergyPlus, in: M. Sjölund, L. Buffoni, A. Pop, L. Ochel (Eds.), Proceedings of the 14th International Modelica Conference, no. 181 in Linköping Electronic Conference Proceedings, Modelica Association and Linköping University Electronic Press, 2021, pp. 325–334. doi:10.3384/ecp21181325.

[56] M. Bonvini, M. Wetter, T. S. Nouidui, A Modelica package for building-to-electical grid integration, in: 5th BauSim Conference, IBPSA-Germany, Aachen, Germany, 2014, pp. 6–13.

[57] International Association for the Properties of Water and Steam, Revised Release on the IAPWS Industrial Formulation 1997 for the Thermodynamic Properties of Water and Steam, Tech. Rep. August, Lucerne, Switzerland (2007).